Optimal design of dual-reflux pressure swing adsorption units via equilibrium theory: process configurations employing heavy gas for pressure swing

Tushar S. Bhatt [a], Giuseppe Storti [b], Joeri F. M. Denayer [a], Renato Rota [c,*]

[a] *Vrije Universiteit Brussel, Department of Chemical Engineering, Pleinlaan 2 , 1050 Brussels, Belgium*

[b] *ETH Zürich, Department of Chemistry and Applied Biosciences, Vladimir-Prelog-Weg 1, HCI F 125, 8093 Zürich, Switzerland*

[c] *Politecnico di Milano, Chemistry, Materials and Chemical Engineering Department "Giulio Natta", Via Mancinelli 7, 20131 Milan, Italy*

HIGHLIGHTS

- An optimal design strategy is presented for the process configuration DR-PL-A.
- Key parameters needed to establish complete separation at CSS are identified.
- An operating window for achieving complete separation at CSS is proposed.
- The influence of process variables (adsorbent selectivity, feed gas composition and, operating pressure ratio) on the design parameters and a novel criterion (that facilitates the choice amongst DR-PL-A and DR-PH-A process cycle configuration) is discussed.

ABSTRACT

Dual-reflux pressure swing adsorption process is theoretically capable of completely separating binary feed gas mixtures into two pure species. The pressure of bed to which the binary gas mixture is fed and the type of gas utilized for pressure swing, results in different process cycle configurations, even if the majority of the previous studies of DR-PSA are restricted to two cycle configurations: that employ heavy gas for pressure swing and deliver feed to the bed operated at either high or low pressure. However, the comparative assessment and the optimal operating pressure ratio of these two process cycle configurations are not well-established. We previously reported an optimal design strategy (that identified a triangular operating zone, inside which, complete separation of binary gas mixtures can be achieved) for one such DR-PSA process cycle configuration. In this work, we report an optimal design strategy for

http://dx.doi.org/10.1016/j.cej.2016.11.111

another DR-PSA process cycle configuration: feed to low pressure bed and pressure swing using heavy gas. With respect to previous literature, the equilibrium theory based comprehensive tracking of the characteristic curves and shock transitions during constant and non-constant pressure steps of this specific cyclic process revealed distinct constraints, design parameter values and boundary conditions of the triangular operating zone. Additionally, an in-depth comparative assessment of the impact of process variables (adsorbent selectivity, feed gas composition and, operating pressure ratio) on the design parameters (optimal feed injection position and ratio of pure light reflux to feed rate) and a novel selection criterion is discussed for both of these cycle configurations in order to (i) facilitate the choice of appropriate cycle configuration and (ii) identify the optimal high to low operating pressure ratio range.

Keywords:

Pressure swing adsorption

Dual-reflux

PSA design

Gas separation

Equilibrium theory

Cyclic adsorption process

Abbreviations: CSS, cyclic steady-state; DR-PH-A, dual-reflux pressure swing adsorption system with feed to the high pressure bed and pressure swing using heavy gas; DR-PL-A, dual-reflux pressure swing adsorption system with feed to the low pressure bed and pressure swing using heavy gas; DR-PH-B, dual-reflux pressure swing adsorption system with feed to the high pressure bed and pressure swing using light gas; DR-PL-B, dual-reflux pressure swing adsorption system with feed to the low pressure bed and pressure swing using light gas; DR-PSA, dual-reflux pressure swing adsorption; TOZ, triangular operating zone.

* Corresponding author. Tel.: +39 0223993154; fax: +39 0223993180.

E-mail address: renato.rota@polimi.it

http://dx.doi.org/10.1016/j.cej.2016.11.111

Nomenclature

A	strongly adsorbed species, heavy product/ component
B	weakly adsorbed species, light product/ component
BD	blowdown step
$Bed-I$	adsorption column depicted in Fig.1
$Bed-II$	adsorption column depicted in Fig.1
C	characteristic
$\mathbb{C}$	capacity ratio of the *purge* step, *dimensionless*
$\mathbb{C}_{Max}$	maximum capacity ratio of the *purge* step, *dimensionless*
CSS	cyclic steady-state
DR-PH-A	dual-reflux pressure swing adsorption system with feed to the high pressure bed and pressure swing using heavy gas
DR-PL-A	dual-reflux pressure swing adsorption system with feed to the low pressure bed and pressure swing using heavy gas
DR-PH-B	dual-reflux pressure swing adsorption system with feed to the high pressure bed and pressure swing using light gas
DR-PL-B	dual-reflux pressure swing adsorption system with feed to the low pressure bed and pressure swing using light gas

http://dx.doi.org/10.1016/j.cej.2016.11.111

DR-PSA	dual-reflux pressure swing adsorption
FE	feed step
$\mathbb{G}$	light recycle ratio stated as the ratio of pure light reflux to feed rate, *dimensionless*
$\mathbb{H}$	dimensionless quantity defined by Eq.(10)
HP	heavy Product
HR	heavy Reflux
L_{bed}	length of each adsorption column, *m*
LP	light Product
LR	light Reflux
N	number of moles, *kmol*
$\dot{N}$	molar flowrate, *kmol/s*
N_{BD}	total amount of gas extracted from the adsorption column during BD, *kmol*
N_{Comp}	total amount of gas that needs to be compressed, *kmol*
$N_{Comp,PS}$	amount of gas that needs to be compressed to achieve pressure swing, *kmol*
$\dot{N}_F$	molar flowrate of binary feed gas mixture, *kmol/s*
N_F	amount of binary feed gas mixture, *kmol*
$N_{F,Max}$	maximum amount of feed gas that can be processed, *kmol*

http://dx.doi.org/10.1016/j.cej.2016.11.111

$\dot{N}_{H,in}$ molar flowrate of heavy reflux, *kmol/s*

$\dot{N}_{H,out}$ molar flowrate of gas released from the adsorption bed undergoing constant high pressure step, *kmol/s*

$\dot{N}_{L,in}$ molar flowrate of light reflux, *kmol/s*

$\dot{N}_{L,out}$ molar flowrate of gas released from the adsorption bed undergoing constant low pressure step, *kmol/s*

N_{PR} total amount of gas transferred to the adsorption column during PR, *kmol*

$\dot{N}_{RS,in}$ molar flowrate of gas entering the *rectifying section* of the column during FE, *kmol/s*

$\dot{N}_{RS,out}$ molar flowrate of gas exiting the *rectifying section* of the column during FE, *kmol/s*

$\dot{N}_{SS,in}$ molar flowrate of gas entering the *stripping section* of the column during FE, *kmol/s*

$\dot{N}_{SS,out}$ molar flowrate of gas exiting the *stripping section* of the column during FE, *kmol/s*

$\mathbb{P}$ pressure ratio (Ratio of high pressure to low pressure), *dimensionless*

P total pressure, or Final pressure, *bar*

P_0 initial pressure, *bar*

P_{Eq} equalization pressure equivalent to: $(P_H + P_L)/2$, *bar*

P_H high pressure, *bar*

P_L low pressure, *bar*

PR pressurization step

http://dx.doi.org/10.1016/j.cej.2016.11.111

PSA	pressure swing adsorption
PU	purge step
R	ideal Gas Constant, *(m^3.bar)/(K.kmol)*
RS	rectifying section
RW	rectifying wave
S	shock
SS	stripping section
SW	stripping wave
T	temperature, *K*
t	time, *s*
t_{cycle}	duration of one DR-PSA cycle, *s*
t_{FE}	duration of *feed* step, *s*
TOZ	triangular operating zone
t_{PU}	duration of *purge* step, *s*
t_{step}	duration of constant or variable pressure step, *s*
V_{bed}	individual bed volume, m^3
y	mole fraction of heavy component, or final composition (in terms of A), or specific concentration value (in terms of A), *dimensionless*

http://dx.doi.org/10.1016/j.cej.2016.11.111

$(1-y)$ mole fraction of light component, *dimensionless*

$\mathbb{Y}(y)$ dimensionless quantity equivalent to: $1+(\beta-1)y$

$(y=0)$ mole fraction of pure light material, *dimensionless*

$(y=1)$ mole fraction pure heavy material, *dimensionless*

y_0 initial composition (in terms of A), *dimensionless*

y_1 composition (in terms of A) at a specific position, mole fraction of heavy component at the leading edge of the shock wave, *dimensionless*

y_2 composition (in terms of A) at a specific position, mole fraction of heavy component at the trailing edge of the shock wave, *dimensionless*

y_F mole fraction of heavy component in binary feed gas mixture, *dimensionless*

y^* mole fraction (in terms of A) of concentration plateau at the end of PR whose concentration (in terms of A) was y_F at the start of PR, *dimensionless*

Z axial co-ordinate normalized with respect to column length, or final position, *dimensionless*

z position along the length of the adsorption column, *m*

$Z=0$ column end from where, light material is either injected-in or is released during the process, *dimensionless*

$Z=1$ column end from where, heavy material is either injected-in or is released during the process, *dimensionless*

Z_0 initial position, *dimensionless*

http://dx.doi.org/10.1016/j.cej.2016.11.111

Z_F feed injection position along the length of the adsorption column, *dimensionless*

$Z_{F,Max}$ maximum limit for feed injection position along the length of the adsorption column, *dimensionless*

$Z_{F,Min}$ minimum limit for feed injection position along the length of the adsorption column, *dimensionless*

$Z_{F,opt}$ optimum feed injection position along the bed length, *dimensionless*

Greek letters

β separation parameter of the adsorbent given by the ratio: (β_A/β_B), *dimensionless*

β_i separation parameter of the adsorbent for species i, *dimensionless*

ε interstitial porosity of the adsorption bed, *dimensionless*

θ time co-ordinate normalized with respect to constant or variable pressure step times, *dimensionless*

Subscripts

0 refers to initial condition or position, pure light composition

$1, 2$ refers to the gas composition (in terms of A) at a specific position, or the gas composition (in terms of A) at the leading and trailing edge of the shock-wave, respectively.

A refers to heavy species

http://dx.doi.org/10.1016/j.cej.2016.11.111

B	refers to light species
BD	refers to *blowdown* step
bed	refers to adsorption column
C	refers to characteristic
$Comp$	refers to the amount of gas that needs to be compressed
$Comp, PS$	refers to the amount of gas that needs to be compressed to achieve pressure swing
Eq	refers to the equalization pressure
F	refers to the composition (in terms of A) of binary feed gas mixture, or feed injection position along the bed length, or the molar flowrate of feed gas mixture, or the molar amount of feed gas mixture
F, Max	refers to the maximum amount of feed gas that can be processed
FE	refers to *feed* step
H	refers to high pressure
H, in	refers to heavy reflux
H, out	refers to gas released from the adsorption bed undergoing constant high pressure step
L	refers to low pressure
L, in	refers to light reflux
L, out	refers to gas released from the adsorption bed undergoing constant low pressure step

http://dx.doi.org/10.1016/j.cej.2016.11.111

Max	refers to the maximum value
Min	refers to the minimum value
opt	refers to the optimum value
PR	refers to *pressurization* step
PU	refers to *purge* step
RS	refers to the *rectifying section*
RS, in	refers to the gas entering the *rectifying section* of the column during FE
RS, out	refers to the gas exiting the *rectifying section* of the column during FE
RW	refers to the rectifying wave
S	refers to shock wave
SS	refers to *stripping section*
SS, in	refers to the gas entering the *stripping section* of the column during FE
SS, out	refers to the gas exiting the *stripping section* of the column during FE
$step$	refers to constant or variable pressure steps
SW	refers to stripping wave

http://dx.doi.org/10.1016/j.cej.2016.11.111

Superscripts

BD, FE	refer to particular locations along the length of the adsorption column at the end of *blowdown* and *feed* steps, respectively
$*$	refers to a specific position along the length of the adsorption column, or the composition (in terms of A) of a specific characteristic, or the gas composition at one of the edges (leading or trailing) of a shock.

http://dx.doi.org/10.1016/j.cej.2016.11.111

1. Introduction

The current recognition of pressure swing adsorption (PSA) technology as the method of choice for the separation and/or purification of many gaseous mixtures can be credited to more than five decades of persistent scientific advancements in the field of adsorption. The development of dual-reflux pressure swing adsorption (DR-PSA) process is one of such prominent scientific advancement. Independently proposed by Hirose [1] and Leavitt [2], DR-PSA process, also termed as *duplex* PSA, is theoretically capable of completely separating binary feed gas mixtures into two pure species, A (strongly adsorbed) and B (weakly adsorbed). DR-PSA systems merge the features of stripping PSA (based on Skarstrom cycle; Skarstrom [3]) and rectifying PSA (also known as enriching reflux PSA; Yoshida et al. [4]) developed by Diagne et al. [5] and Ebner and Ritter [6]. An integrated two-bed system, each possessing an intermediate port for feed injection in position Z_F along the axis, is representative of a DR-PSA unit. Such feed injection port splits each adsorption bed in two sections: the '*Stripping Section*' (SS), before the feed in the direction of the gas flow, and the '*Rectifying Section*' (RS). At complete separation, two reflux streams, light reflux (LR, pure B), and heavy reflux (HR, pure A), are respectively injected at the SS and RS end of each bed during constant pressure steps.

In a DR-PSA unit, binary feed gas can be delivered to the bed operated at high (P_H) or low pressure (P_L) and pressure swing can be carried out either with pure A or B species. Kearns and Webley [7] explored this flexibility and proposed four distinct DR-PSA cycle configurations: (i) DR-PH-A: Feed to P_H and pressure swing with A; (ii) DR-PL-A: Feed to P_L and pressure swing with A; (iii) DR-PH-B: Feed to P_H and pressure swing with B, and; (iv) DR-PL-B: Feed to P_L and pressure swing with B. Although complete separation of binary feed gas mixture is theoretically possible in all of these process cycle configurations, majority of experimental and/or modeling studies of DR-PSA till date are restricted to the two process cycle configurations that employ heavy gas for pressure swing (namely, DR-PH-A and DR-PL-A), as evident from the subsequent survey.

http://dx.doi.org/10.1016/j.cej.2016.11.111

Separation and/or purification of gaseous mixtures in laboratory-scale DR-PSA process units have been reported by various authors. Diagne et al. [5, 8, 9] demonstrated CO_2 separation from air using zeolite 13X in DR-PH-A and DR-PL-A process cycle configuration. The recovery and enrichment of dilute ethane from nitrogen using MeadWestvaco BAX-1500 activated carbon in DR-PL-A configuration was reported by McIntyre and coworkers [10, 11]. The laboratory-scale experimental study by Bhatt et al. [12] demonstrated the concentration of dilute gaseous feed of methane in nitrogen using Norit RB1 activated carbon in DR-PH-A cycle configuration. The experimental study by Saleman and coworkers [13] showed the separation of methane and nitrogen feed gas mixture into a high purity nitrogen and an enriched methane product stream, by means of Norit RB3 activated carbon and DR-PL-A cycle configuration. Utilizing silica gel as adsorbent, Li et al. [14] reported the separation of CO_2 and N_2 mixture in a laboratory-scale unit that employed DR-PH-A and two altered forms of DR-PSA process cycle configurations: feed to high pressure bed and pressure swing with gas streams enriched with both heavy and light components.

In order to design, optimize and/or simulate DR-PSA process, mathematical models with different levels of complexity are also reported in literature. A comprehensive (or "detailed") model generally considers: non-linear and competitive adsorption isotherms, mass transport resistances, non-ideal gas behavior, axial and/or radial dispersions, pressure and/or temperature gradients. Similar models have been utilized by various authors to perform process simulations. Diagne and coworkers [15] used a detailed model to simulate their experiments that employed DR-PL-A process cycle configuration. A detailed model was employed by Spoorthi et al. [16] and Thakur et al. [17] to demonstrate their process intensification studies via simulation of DR-PH-B and a modified version of DR-PH-B cycle configuration. In addition to these cycle configurations, DR-PH-A configuration was simulated by means of a detailed model by Sivakumar and Rao [18, 19] to make evident their improvements in process performance. Using detailed model developed in the frame of the commercial software Aspen Adsim®, Bhatt and coworkers [12] elucidated DR-PSA process behavior that employed DR-PH-A cycle configuration. Such detailed models were also employed by Bhatt

http://dx.doi.org/10.1016/j.cej.2016.11.111

et al. [20] to simulate the experiments performed by McIntyre and coworkers [11] in DR-PL-A cycle configuration and by Zhang et al. [21] to simulate the experiments reported by Saleman and coworkers [13] again in DR-PL-A cycle configuration.

Equilibrium theory, a simplified modeling approach (Rhee et al., [22]), assumes: instantaneous equilibrium between the two phases, ideal gas behavior, ideal plug flow, isothermal operation, and zero pressure drop. Analytical solutions of such model equations have been reported in the case of linear adsorption equilibria only. Namely, Ebner and Ritter [23] examined the effect of changing the feed position Z_F between a minimum ($Z_{F,Min}$) and a maximum value ($Z_{F,Max}$) in DR-PL-A cycle configuration. Later on, Kearns and Webley [7] used equilibrium theory to propose a specific feed position and reflux rate that ensured maximum adsorbent utilization in each of the four cycle configurations (DR-PH-A, DR-PL-A, DR-PH-B and, DR-PL-B). This simplified modeling approach was most recently utilized by Bhatt et al. [24] to propose an optimal design strategy for DR-PH-A cycle configuration.

The aforementioned literature survey revealed that majority of the researchers used either DR-PH-A or DR-PL-A process cycle configuration for their experimental and/or modeling analysis, without clearly stipulating the motivation for such selection. Kearns and Webley [25] provide the only available guideline for such a choice based on their productivity and energy consumption criteria. However, the same authors averred that their investigations were not aimed at establishing the optimal high to low operating pressure ratio. Since energy consumption is directly related to the operating pressure ratio; identification of an optimal value of such a significant process parameter would have further assisted the practicing engineer in achieving maximum process performance.

On the basis of equilibrium theory and with the major assumption of linear adsorption equilibrium, an optimal design procedure for DR-PSA units was proposed by Bhatt et al. [24]. Albeit the fact that their simplistic modeling approach fully neglected mass transport resistances, it provided some unique insights

http://dx.doi.org/10.1016/j.cej.2016.11.111

with respect to previous literature. Although this optimal design procedure is applicable to other DR-PSA process cycle configurations, the authors restricted their study to the specific configuration DR-PH-A. Moreover, no attempt was made by even these authors to establish an optimal high to low operating pressure ratio range.

Such inadequacies found in previous literatures became the key motivation for our current quest. Once more limiting ourselves to linear adsorption equilibrium, in this work we apply equilibrium theory to another DR-PSA process cycle configuration, DR-PL-A, with the intent of accomplishing the following objectives:

(i) provide an optimal design procedure for DR-PL-A process cycle configuration;

(ii) develop a correlation between the single specific value of Z_F proposed by Kearns and Webley [7] and the range of values for the same variable ($Z_{F,Min}$ to $Z_{F,Max}$) put forth by Ebner and Ritter [23] for achieving complete separation of binary feed gas mixtures in DR-PL-A process cycle configuration;

(iii) facilitate the selection between DR-PL-A and DR-PH-A cycle configuration based on process variables, and;

(iv) establish the optimal high to low operating pressure ratio range for both (DR-PL-A and DR-PH-A) process cycle configurations.

Future work will deal with the optimal design and comparative assessment of DR-PSA process cycle configurations that employ light gas for pressure swing (DR-PH-B and DR-PL-B).

2. Methods

2.1. DR-PL-A process cycle description

The schematic diagram of a typical twin-bed DR-PL-A process cycle configuration (under the assumption of complete separation at CSS) is shown in Fig. 1. In this particular configuration, each of the two identical

http://dx.doi.org/10.1016/j.cej.2016.11.111

adsorption beds ($Bed-I$ and $Bed-II$) run through a four step cyclic process: two steps are simultaneously executed at constant pressure and remaining two at non-constant pressure. Note that in Fig. 1, only half-cycle is illustrated since the same steps occur with the column numbers transposed. As anticipated, the feed injection position along the bed, defined as Z_F in terms of normalized axial coordinate ($Z = z/L_{bed}$), divides each bed into two sections, the stripping section ($Z < Z_F$; SS) and the rectifying section ($Z > Z_F$; RS). Pure B ($y = 0$; mole fraction of heavy component is referred to as y) is either injected-in or pushed-out of the end of SS, $Z = 0$, while pure A ($y = 1$) is either injected-in or pushed-out of the end of RS, $Z = 1$.

Binary feed gas mixture with flowrate $\dot{N}_F$ and composition y_F (mole fraction of A in feed) is supplied to $Bed-I$ which is maintained at constant pressure equal to P_L during the *feed* step (FE); simultaneously, $Bed-II$ undergoes *purge* step (PU) while being maintained at constant P_H. Pure A ($y = 1$) is pushed out of the $Bed-I$ at flowrate $\dot{N}_{L,out}$, a portion of which is taken out of the system as Heavy Product (HP) with flowrate $\dot{N}_F y_F$ and the remaining portion is compressed and supplied as Heavy Reflux (HR) to $Bed-II$ (undergoing PU) at flowrate $\dot{N}_{H,in}$. Pure B ($y = 0$) exits from $Bed-II$ at flowrate $\dot{N}_{H,out}$, a portion of which is taken out of the system as Light Product (LP) at flowrate $\dot{N}_F(1-y_F)$ and the remaining quantity is supplied to $Bed-I$ as Light Reflux (LR) at flowrate $\dot{N}_{L,in}$.

At the end of the simultaneous FE/PU, the bed pressures need to be interchanged. This is accomplished by transferring pure A ($y = 1$) gas from the rectifying end ($Z = 1$) of $Bed-II$ to the $Z = 1$ end of $Bed-I$ (after compression). Hence, $Bed-II$ undergoes *blowdown* step (BD) during which its pressure decreases from P_H to P_L and, simultaneously, $Bed-I$ undergoes *pressurization* step (PR) during which its pressure increases from P_L to P_H. The total amounts of gas extracted from $Bed-II$ and transferred to $Bed-I$ during these steps are indicated as N_{BD} and N_{PR}, respectively.

http://dx.doi.org/10.1016/j.cej.2016.11.111

2.2. Equilibrium model

The equilibrium theory based model used in this work is identical to the one reported by Bhatt et al. [24]. Accordingly, we retain (i) model assumptions, (ii) meaning, notations and units of variables, and (iii) constitutive model equations as outlined in the mentioned paper. Therefore, the model is not restated here to avoid repetitions.

2.3. Mathematical formulations for DR-PL-A process cycle configuration

In order to accomplish the complete separation of binary feed gas mixture at cyclic steady state (CSS) conditions, the simulation of the four-step DR-PL-A cycle is carried out through an equilibrium model adapted from the one proposed by Bhatt et al. [24] for another process configuration. Namely, two main representations of the solution will be discussed: (i) the concentration profiles along the column as a function of time (represented in Fig. 2), and (ii) the "topology" of the solution, i.e. the depiction of the different transitions and constant states of composition in the space-time plane (represented in Fig. 3). In both of these representations, the time and/or pressure evolutions along the column length during the four-step DR-PL-A cycle are depicted for a single column; for complete separation at CSS, these depictions apply to both columns. Note that the vertical coordinate, Cycle Time $\left(t_{cycle}\right)$, in Fig. 3 is actually the time during the constant pressure steps, FE and PU, and is the pressure during the variable pressure steps, BD and PR. Moreover, each time or pressure interval has been normalized to the step duration or to the pressure change in order to have the same vertical size for the four process steps. Some arrows are reported in Fig. 2 to indicate inlet or outlet molar flowrates $\left(\dot{N}\right)$ or molar quantities (N). For complete separation at CSS, such amounts have to fulfill the following requirements (Bhatt et al., [24]):

$$N_{BD} = \frac{\varepsilon V_{bed}(P_H - P_L)}{RT\beta_A} = N_{PR} \tag{1}$$

http://dx.doi.org/10.1016/j.cej.2016.11.111

$$\dot{N}_{L,out} = \frac{\dot{N}_{L,in} + \dot{N}_F \mathbb{Y}(y_F)}{\beta} \tag{2}$$

$$\dot{N}_{H,out} = \dot{N}_{L,in} + \dot{N}_F(1 - y_F) \tag{3}$$

$$\dot{N}_{H,in} = \frac{\dot{N}_{H,out}}{\beta} \equiv \frac{\dot{N}_{L,in} + \dot{N}_F(1 - y_F)}{\beta} \tag{4}$$

$$t_{FE} = t_{PU} \tag{5}$$

where ε (interstitial porosity of the adsorbent bed), V_{bed} (adsorbent bed volume), R (ideal gas constant), T (gas temperature), β_A (separation parameter of the adsorbent for species A), β (separation parameter of the adsorbent), y_F (mole fraction of heavy component in binary feed gas mixture), t_{FE} (duration of *feed* step) and t_{PU} (duration of *purge* step) hold the same definition and dimensions as outlined by Bhatt et al. [24]. Note that in Eq.(2) $\mathbb{Y}(y_F) = 1 + (\beta - 1)y_F$. Given their mathematical form, the characteristics will diverge (thereby causing simple spreading waves) during the *blowdown* (BD) and *feed* (FE) steps. On the other hand, the characteristics will converge, causing self-sharpening waves (that may eventually result in the formation of shock waves) during *pressurization* (PR) and *purge* (PU) steps. Hence, it will be convenient to analyze the DR-PL-A process cycle with step sequence $BD \rightarrow FE \rightarrow PR \rightarrow PU$.

To construct the cycle representation in Fig. 2 and 3, the final composition profile that characterizes the end of the *purge* step is utilized as initial composition profile for the *blowdown* step. It consists of binary constant states $y = y^*$ and $y = 1$ separated by a step change at the position Z^*. The concentration value y^* can be computed via the following equation:

$$\frac{y_F}{y^*} = \left(\frac{1 - y_F}{1 - y^*}\right)^{\beta} (\mathbb{P})^{1-\beta} \tag{6}$$

http://dx.doi.org/10.1016/j.cej.2016.11.111

where $\mathbb{P}$ represents the high to low pressure ratio defined as:

$$\mathbb{P} = \frac{P_H}{P_L} \tag{7}$$

During BD, the concentration plateau initially at $y = y^*$ is becoming wider and reaching the final concentration value y_F. On the other hand, the initial plateau corresponding to pure A $(y = 1)$ shrinks, keeping constant the mole fraction value at 1. Note that, the leftmost step (at the specific position $Z = 0$) doesn't move since this column end is closed during BD. The initial step at Z^* spreads itself in a wave defined as *Rectifying wave* (RW): the final left and right values of the corresponding limiting mole fractions are y_F and 1, respectively. The final positions of $y = 1$ and y_F characteristics (at the end of BD) in RW were evaluated through the equilibrium model and they are represented by Eq.(8) and Eq.(9), respectively:

$$Z_{RW,1}^{BD} = Z^*(\mathbb{P})^{1/\beta} \tag{8}$$

$$Z_{RW,y_F}^{BD} = Z^*(\mathbb{H})^{-1} \equiv Z_{RW,1}^{BD}\left[\mathbb{H}(\mathbb{P})^{1/\beta}\right]^{-1} \tag{9}$$

Such positions have been defined as $Z_{RW,1}^{BD}$ and Z_{RW,y_F}^{BD} , where the superscript indicates the end of the corresponding process step and the subscripts are the wave type and the concentration value, respectively. This same notation has been applied to other special positions shown in Fig. 2 and 3 and discussed below. In Eq.(9), the definition of the dimensionless quantity $(\mathbb{H})$ is kept identical to the one reported by Bhatt et al. [24] and it is restated below to avoid ambiguity.

$$\mathbb{H} = \left(\frac{y^*}{y_F}\right)^{\beta/(1-\beta)} \left(\frac{1-y_F}{1-y^*}\right)^{1/(1-\beta)} \frac{\mathbb{Y}(y^*)}{\mathbb{Y}(y_F)} \tag{10}$$

The next *feed* step is running at constant, low pressure and with a duration of t_{FE}: $\dot{N}_{L,in}$ enters with composition $y = 0$ at $Z = 0$, $\dot{N}_F$ enters with composition y_F at $Z = Z_F$, and $\dot{N}_{L,out}$ exits at the other end of the column ($Z = 1$), with composition $y = 1$. All these flowrates are linked together through Eq.(2). Part of $\dot{N}_{L,out}$ is taken out of the system as heavy product (under the assumption of complete separation at CSS, its flowrate is equal to $\dot{N}_F y_F$) and the remaining part $\dot{N}_{H,in}$ is supplied at $Z = 1$ end of the other column as heavy recycle during the high pressure *purge* step. The inlet (in) and outlet (out) molar flowrates of each section of the column are readily expressed as follows:

Stripping Section (SS):

$$\dot{N}_{SS,in} = \dot{N}_{L,in} \tag{11}$$

$$\dot{N}_{SS,out} = \frac{\dot{N}_{L,in}}{\mathbb{Y}(y_F)} \tag{12}$$

Rectifying Section (RS):

$$\dot{N}_{RS,in} = \frac{\dot{N}_{L,in} + \dot{N}_F \mathbb{Y}(y_F)}{\mathbb{Y}(y_F)} \tag{13}$$

$$\dot{N}_{RS,out} = \dot{N}_{L,out} \tag{14}$$

Since the adsorption column is at constant, low pressure during FE, using the aforementioned flowrates and their respective compositions as reference, the following equations can be employed to calculate the trajectories of the characteristics in different sections of the bed:

Stripping Section (SS):

$$\left.\frac{dZ}{d\theta}\right|_{SS,C} = \frac{\mathbb{C}}{\mathbb{Y}^2(y)} \tag{15}$$

http://dx.doi.org/10.1016/j.cej.2016.11.111

Rectifying Section (RS):

$$\left.\frac{dZ}{d\theta}\right|_{RS,C} = \frac{\mathbb{C}[1 + \mathbb{Y}(y_F)\mathbb{G}^{-1}]}{\mathbb{Y}^2(y)} \tag{16}$$

where $\mathbb{Y}(y) = 1 + (\beta - 1)y$ and $\theta = t/t_{step}$. The definitions of the two parameters $\mathbb{C}$ (capacity ratio of the *purge* step) and $\mathbb{G}$ (ratio of pure light reflux to feed rate) are identical to those reported by Bhatt et al. [24] but restated below to avoid ambiguity.

$$\mathbb{C} = \frac{\beta_A \dot{N}_{L,in} t_{FE} RT}{P_L V_{bed} \varepsilon} \equiv \frac{\beta_A RT\mathbb{G}}{P_L \varepsilon} \quad \frac{N_F}{V_{bed}} \tag{17}$$

$$\mathbb{G} = \frac{\dot{N}_{L,in}}{\dot{N}_F} \tag{18}$$

Since at constant pressure the composition is constant all along the characteristics, Eq. (15) and (16) can be readily integrated and their integrated forms are stated as Eq. (19) and (20), respectively:

Stripping Section (SS):

$$(Z - Z_0)|_y = \frac{\mathbb{C}}{\mathbb{Y}^2(y)} \tag{19}$$

Rectifying Section (RS):

$$(Z - Z_0)|_y = \frac{\mathbb{C}[1 + \mathbb{Y}(y_F)\mathbb{G}^{-1}]}{\mathbb{Y}^2(y)} \tag{20}$$

where Z_0 and Z represent the initial and final position of a specific concentration value (y). During FE, the initial leftmost step at $Z = 0$ spreads itself in a wave defined as *Stripping wave* (SW). Since the composition of SW is constant all along the characteristics, the final left and right values of the

http://dx.doi.org/10.1016/j.cej.2016.11.111

corresponding limiting mole fractions are $y = 0$ and y_F, respectively. The final position of y_F characteristic at the end of FE in SW can be readily evaluated through Eq.(19):

$$Z_{SW,y_F}^{FE} = \frac{\mathbb{C}}{\mathbb{Y}^2(y_F)} \tag{21}$$

Also during FE, RW shifts forward towards the column end $Z = 1$. The final position of the limiting concentration $y = 1$ of RW at the end of the *feed* step can be readily evaluated through Eq. (20) as follows:

$$Z_{RW,1}^{FE} - Z_{RW,1}^{BD} = \frac{\mathbb{C}[1 + \mathbb{Y}(y_F)\mathbb{G}^{-1}]}{\beta^2} \tag{22}$$

During the pressure changing PR step, the $Z = 0$ end of the bed is closed, N_{PR} moles of pure heavy gas enters the column at $Z = 1$ and the pressure of the entire column increases from P_L to P_H. Due to the reinjection of heavy component through the right end of the column, both waves turn to the left ($Z = 0$ end of the column) and the intermediate constant state initially at y_F changes its plateau value finally to y^*. Under these conditions, the characteristics converge, causing self-sharpening and eventually developing shock (S) waves. Depending on the specific parameter values and operating conditions, shocks may form in the SW and/or RW. The trajectory of characteristics and the propagation of shock waves formed by characteristic superposition can be numerically evaluated once more using the equilibrium model equations (cf. Rhee et al. [22]; Kearns and Webley [7]; Bhatt et al. [24]). An effective, numerical approach based on direct check of the superposition of adjacent characteristics has been applied in this work. It is closely resembling the approach previously applied by Bhatt et al. [24] and it is shortly summarized in the *Appendix A*. Notably, shock formation can start everywhere in the RW, including intermediate concentration values; on the other hand, the shock formation in the SW always starts at the highest limiting concentration value. This different behavior reflects the different wave spreading during

http://dx.doi.org/10.1016/j.cej.2016.11.111

the first, variable pressure step of the cycle (BD): while SW doesn't spread at all, the concentration profile in RW can be very heterogeneous, depending upon the specific operating conditions. Such heterogeneity makes possible the first superposition of characteristics (i.e. the beginning of shock development) at any concentration value inside the RW.

Let us finally consider the *purge* step, PU. This is a constant, high pressure step with part of the heavy component recovered (during FE) from the other column injected at the $Z = 1$ end of the column under consideration (flowrate $\dot{N}_{H,in}$), whereas pure light component exits the opposite ($Z = 0$) column end (flowrate $\dot{N}_{H,out}$), being the flowrates linked together through Eq.(4). Part of $\dot{N}_{H,out}$ is taken out of the system as light product (under the assumption of complete separation, its flowrate is equal to $\dot{N}_F(1 - y_F)$) and the remaining part $\dot{N}_{L,in}$ is supplied at $Z = 0$ end of the other column as light recycle during the low pressure *feed* step. The trajectories of characteristics (C) and shocks (S) can be evaluated using the following equations:

$$\left.\frac{dZ}{d\theta}\right|_C = \frac{\mathbb{C}}{\mathbb{Y}^2(y)}\left[\frac{(y_F - 1)}{\mathbb{G}} - 1\right]\frac{1}{\mathbb{P}} \tag{23}$$

$$\left.\frac{dZ}{d\theta}\right|_S = \frac{\mathbb{C}}{\mathbb{Y}(y_1)\mathbb{Y}(y_2)}\left[\frac{(y_F - 1)}{\mathbb{G}} - 1\right]\frac{1}{\mathbb{P}} \tag{24}$$

In Eq.(24), the subscripts 1 and 2 refer to the composition at the leading and trailing edge of the shock wave, respectively. Note that, the leading edge composition of the shock in the SW will always be equivalent to y^* (highest limiting concentration value).

After identifying the positions of shock formation and its complete development (complete shock development in the SW and RW is depicted by small circles in Fig. 3), the calculation of the space-time

http://dx.doi.org/10.1016/j.cej.2016.11.111

evolutions of both the transitions can be numerically done using the concentration profiles calculated at the end of the previous process step as initial conditions.

To summarize, the equilibrium model of the process reduces to the equations introduced above for evaluating the topology of the solution in each step. Such equations can be solved sequentially step by step, using the final conditions of one step as initial conditions for the following one, to provide the complete picture, composition-space-time, of the DR-PL-A process for complete separation at CSS. To calculate the solution, the values of the following 7 parameters are needed: separation parameter of the adsorbent (β), feed composition (y_F), pressure ratio ($\mathbb{P}$), feed position (Z_F), initial position of RW (Z^*), capacity ratio of the *purge* step ($\mathbb{C}$), and light recycle ratio ($\mathbb{G}$).

Note that, in order to ensure complete separation at CSS at given values of $\beta, y_F, \mathbb{P}, \mathbb{C}$, and $\mathbb{G}$, the specific value of the positions Z_F and Z^* are interdependent. In other words, if the value of one of these positions (say, Z_F) is evaluated, the value of the other interdependent position (Z^*) gets defined by design (for complete separation at CSS). Such interdependency of Z_F and Z^* is elaborated in the forthcoming discussion.

2.4. Optimal solution – Triangular Operating Zone (TOZ) for DR-PL-A process cycle configuration

In general, given separation parameter of the adsorbent, feed composition and pressure ratio, the remaining 4 process parameters ($Z_F, Z^*, \mathbb{C}$, and $\mathbb{G}$) have to be evaluated in order to fulfill properly all the constraints needed to establish complete separation at CSS. With reference to the topology of the solution provided in Fig. 3, three positions which are key to define the separation are: Z^{BD}_{RW,y_F} , $Z^{FE}_{RW,1}$, and Z^{FE}_{SW,y_F}.

For complete separation, the values of these positions as well as the initial positions of both the *Stripping* and *Rectifying waves* have to fulfill the following constraints:

http://dx.doi.org/10.1016/j.cej.2016.11.111

1. The maximum value of Z_{RW,y_F}^{BD} (position of leftmost composition in the *Rectifying wave* at the end of BD) cannot be smaller than the feed position ($Z_{RW,y_F}^{BD} \geq Z_F$) in order to ensure feed injection inside a constant state at $y = y_F$, thus preventing any change in composition of the intermediate constant state.

2. The rightmost characteristic ($y = 1$) of RW at the end of FE cannot leave the column, meaning that its final position, $Z_{RW,1}^{FE}$, cannot be larger than 1 ($Z_{RW,1}^{FE} \leq 1$).

3. The maximum value of Z_{SW,y_F}^{FE} (position of rightmost composition in the *Stripping wave* at the end of FE) cannot be larger than the feed position ($Z_{SW,y_F}^{FE} \leq Z_F$) in order to ensure feed injection inside a constant state at $y = y_F$, thus preventing any change in composition of the intermediate constant state.

4. At the end of *purge* step, both the *Stripping* and *Rectifying waves* have to "shrink" into fully developed shocks (SW: $y_1 = y^*$, $y_2 = 0$; RW: $y_1 = 1$, $y_2 = y^*$) and should reach $Z = 0$ end of the column and the specific position Z^*, respectively. This way, the concentration profile considered as initial condition for the *BD* step is actually achieved.

The first three inequalities can be used to evaluate feasible range of values of starting position of RW (Z^*), feed position (Z_F), and capacity ratio of the *purge* step ($\mathbb{C}$); on the other hand, the last requirement is used to determine the last quantity, light recycle ratio ($\mathbb{G}$). Note that *a single value* of $\mathbb{G}$ applies in order to fulfill such constraint whatever the values of the remaining 3 parameters are at conditions of complete separation. The physical meaning of this convenient property is identical to the one reported by Bhatt et al. [24]. Moreover, since the parameter $\mathbb{H}$ is a function of y_F, β and $\mathbb{P}$ (cf. Eq.(6) and (10)), it also remains constant inside the same operating region, i.e. for all set of $(Z_F, Z^*, \mathbb{C})$ values that ensure complete separation at CSS.

http://dx.doi.org/10.1016/j.cej.2016.11.111

Following the discussion above, the evaluation of the four process parameters has been carried out through the following iterative approach:

1. A value of $\mathbb{G}$ is initially guessed.
2. Taking advantage of the first three constraints above, a 3D operating region in the space $(Z_F, Z^*, \mathbb{C})$ suitable for complete separation at CSS is identified. Inside such region, any combination of the three parameters is suitable for complete separation, even though at different efficiency, i.e. asking for different amounts of adsorbent.
3. The correctness of the guessed value of $\mathbb{G}$ is checked by solving the problem through the complete equilibrium model and verifying that CSS conditions are actually established. If not, the value of this parameter is adjusted and the procedure is iterated from point 2.

Let us focus on point 2. above. It can be better understood by specifying the various constraints and taking advantage of the previous Eq.(9), (21) and (22):

$$Z^{BD}_{RW,y_F} \equiv Z^*(\mathbb{H})^{-1} \geq Z_F \tag{25}$$

$$Z^{FE}_{RW,1} \equiv Z^*(\mathbb{P})^{1/\beta} + \frac{\mathbb{C}}{\beta^2}(1 + \mathbb{Y}(y_F)\mathbb{G}^{-1}) \leq 1 \tag{26}$$

$$Z^{FE}_{SW,y_F} \equiv \frac{\mathbb{C}}{\mathbb{Y}^2(y_F)} \leq Z_F \tag{27}$$

Given the value of the parameter $\mathbb{G}$, these 3 inequalities with the three variables $(Z_F, Z^*, \mathbb{C})$ define the 3D operating region mentioned above. Such region is qualitatively depicted in Fig. 4a in the space $(Z_F - Z^* - \mathbb{C})$. It is a tetrahedron with triangular base (right-angled triangle), six edges, three triangular faces (one straight and two inclined), and four vertex corners.

Once defined the region of complete separation in terms of operating parameters, it is worth identifying the optimal conditions inside such region. In order to evaluate the process optimality, the parameter $\mathbb{C}$ is

http://dx.doi.org/10.1016/j.cej.2016.11.111

especially relevant. In fact, at constant β, y_F and $\mathbb{P}$, and inside the complete separation region (i.e., at constant $\mathbb{G}$ value), it is directly proportional to the specific adsorbent use (N_F/V_{bed}). Consequently, it can be considered the objective function of our process optimization, to be maximized in order to minimize the solid requirement per mole of feed. Therefore, the surface of the tetrahedral region in Figure 4a represents the locus of all optimal operating points for a given (Z_F, Z^*) pair of values and the absolute optimum is represented by the apex of the tetrahedron.

From Fig.4a, it is clear that the limiting values of $\mathbb{C}$ are located at the ascending edges of the three triangular faces (one straight and two inclined) of the tetrahedron. Such limiting values of $\mathbb{C}$ form the contour line within the triangular region depicted in Fig.4b in the plane ($Z_F - Z^*$). Note that Fig.4b actually represents the top view of the tetrahedron. It can also be directly evaluated by assuming the equality $Z^*(\mathbb{H})^{-1} = Z_F$, defined by constraint (25) above. Utilizing the same equality, constraint (26) can be re-written as:

$$Z_{RW,1}^{FE} \equiv Z_F \mathbb{H}(\mathbb{P})^{1/\beta} + \frac{\mathbb{C}}{\beta^2}(1 + \mathbb{Y}(y_F)\mathbb{G}^{-1}) \leq 1 \qquad (28)$$

This way, the most informative separation region in the plane ($Z_F, \mathbb{C}$) is obtained, shown in Figure 5. As previously obtained for the DR-PH-A configuration (Bhatt et al., [24]), this region has triangular shape and will be termed as Triangular Operating Zone, TOZ: it is determined by the two straight lines given by inequalities (27) and (28) at their maximum values, keeping in mind that Z^* is a function of Z_F.

From Fig. 5 it becomes clear that optimal conditions correspond to the vertex of the triangular region. Such optimal operating point is defined by the intersection of the two straight lines (27) and (28), and the corresponding optimal values of the two parameters Z_F and $\mathbb{C}$ can be readily expressed as follows:

http://dx.doi.org/10.1016/j.cej.2016.11.111

$$Z_{F,opt} = \left\{ \frac{\mathbb{Y}^2(y_F)[1 + \mathbb{Y}(y_F)\mathbb{G}^{-1}]}{\beta^2} + \mathbb{H}(\mathbb{P})^{1/\beta} \right\}^{-1} \tag{29}$$

$$\mathbb{C}_{Max} = Z_{F,opt}\mathbb{Y}^2(y_F) \tag{30}$$

Note that $Z_{RW,1}^{FE} = 1$, $Z_{SW,y_F}^{FE} = Z_{RW,y_F}^{BD} = Z_{F,opt}$, and, as limiting value of inequality (25), $Z^* = \mathbb{H}\, Z_{F,opt}$ at optimal operating conditions (top vertex of the TOZ). At constant β, y_F and $\mathbb{P}$, the parameter $\mathbb{C}$, defined by Eq.(17), is directly proportional to the specific adsorbent use (N_F/V_{bed}). Consequently, $\mathbb{C}_{Max}$ corresponds to the minimum solid requirement per mole of feed. This convenient property allows us to evaluate the maximum amount of feed $N_{F,Max}$ that can be processed while operating the system at $Z_{F,opt}$ and $\mathbb{C}_{Max}$:

$$N_{F,Max} = \frac{P_L V_{bed}\varepsilon}{\beta_A RT} \quad \frac{\mathbb{C}_{Max}}{\mathbb{G}} \tag{31}$$

To conclude this section, the main features of the TOZ can be further summarized:

1. The range of feed positions is decreasing at increasing values of capacity ratio of the *purge* step;
2. The optimal conditions correspond to the top vertex of the region, where the capacity ratio of the *purge* step is maximum ($\mathbb{C} = \mathbb{C}_{Max}$) and $Z_F = Z_{F,opt}$;
3. Given the linear constraints, the operating region has triangular shape (consequently termed as Triangular Operating Zone: TOZ) that can be readily identified from the values of $Z_{F,opt}$, $\mathbb{C}_{Max}$, $\mathbb{H}$, $\mathbb{P}$ and β;
4. A clear correlation between the single specific Z_F proposed by Kearns and Webley [7] and the range for the same variable ($Z_{F,Min}$ to $Z_{F,Max}$) put forth by Ebner and Ritter [23] for achieving complete separation of binary feed gas mixtures in DR-PL-A process cycle configuration can be established via the TOZ.
5. The maximum and minimum limit of Z_F can be deduced by employing $\mathbb{C} = 0$ in Eq.(28) and (27) respectively.

http://dx.doi.org/10.1016/j.cej.2016.11.111

6. A *single* value of $\mathbb{G}$ and $\mathbb{H}$ applies for all pair of $(Z_F - \mathbb{C})$ values inside the TOZ.
7. Process operation for all pair of $(Z_F - \mathbb{C})$ values chosen from the TOZ will achieve complete separation at CSS. However, maximum utilization of the adsorbent can only be achieved when the process is operated at $Z_{F,opt}$ and $\mathbb{C}_{Max}$.
8. Process operation for *any* pair of $(Z_F - \mathbb{C})$ values laying *outside* the TOZ will *not* achieve complete separation at CSS. This also implies that, complete separation at CSS will only be achievable if the correct combination of $Z_F - Z^* - \mathbb{C}$ laying *within* the tetrahedron depicted in Fig. 4a is chosen.

Note that, the optimal conditions correspond to a single, specific value of the feed position, an impractical condition because it is extremely sensitive to any change of operating conditions. To increase the process robustness, a range of feed positions would be welcome and, according to Fig. 5, this can be indeed achieved at expense of a larger demand in terms of solid use.

3. Results and discussion

3.1. Process performances at different operating conditions inside the TOZ

Optimal design strategy of DR-PSA units that employ DR-PL-A process cycle configuration can be demonstrated by evaluating the triangular operating zone at given values of y_F, β and $\mathbb{P}$, and performing simulations at different values of the operating parameters $(Z_F, Z^*, \mathbb{C}, \mathbb{G})$ using the numerical code shortly described in the *Appendix A*. This is fully analogous to the approach previously reported by Bhatt et al. [24] and, therefore, these results are available in *Appendix B*.

3.2. Comparative assessment of DR-PL-A and DR-PH-A process cycle configurations

The practical significance of pressure equalization step (to save on compression energy) in DR-PSA process operation has been emphasized by Kearns and Webley [7]. Pressure equalization can be accomplished in

http://dx.doi.org/10.1016/j.cej.2016.11.111

both DR-PL-A and DR-PH-A process cycle configurations by connecting the heavy gas ends of both the columns via an equalization valve, from the start of PR or BD until equalization pressure $\left(P_{Eq}\right)$ is achieved (cf. Kearns and Webley [7]). Hence, the actual amount of gas that needs to be compressed to achieve the pressure swing is the gas released from the column undergoing BD, *only* while its pressure changes from P_{Eq} to P_L. In the frame of general description of this section, let us define the equalization pressure as reported by Chiang [26]:

$$P_{Eq} = \left(\frac{P_H + P_L}{2}\right) \tag{32}$$

The type (pure A: $y = 1$) and amount ($N_{PR} \equiv N_{BD}$) of gas that needs to be transferred from one column to another for accomplishing the pressure swing in both DR-PL-A (this work: Eq.(1)) and DR-PH-A (Bhatt et al., [24]) configurations is identical. This convenient property (accompanied with the fact that the equilibrium model used here as well as by Bhatt et al. [24] is based on linear adsorption isotherms) allows us to deduce the *actual* amount of gas that needs to be compressed ($Comp$) to achieve the Pressure Swing (PS):

$$N_{Comp,PS} = \frac{\varepsilon V_{bed}\left(P_H - P_{Eq}\right)}{RT\beta_A} \equiv \frac{N_{PR}}{2} \tag{33}$$

Another quantity of gas that needs to be compressed in both of these configurations is $N_{H,in}$ (i.e., the heavy reflux of pure A that needs to be supplied to the column undergoing the constant high pressure step). As mentioned earlier, the definition of $\mathbb{G}$ (ratio of pure light reflux to feed rate) used in this work (for DR-PL-A) is identical to the one reported by Bhatt et al. [24] for DR-PH-A. Correlating the distinct amount of heavy reflux for DR-PH-A and DR-PL-A with the common definition of $\mathbb{G}$, individual values of $N_{H,in}$ can be calculated for both of these process cycle configurations when $N_{F,Max}$ is processed:

http://dx.doi.org/10.1016/j.cej.2016.11.111

$$N_{H,in} = \left[\frac{\mathbb{G} + (1 - y_F)}{\beta}\right] N_{F,Max} \qquad \text{for DR-PL-A} \qquad (34)$$

$$N_{H,in} = \left[\left(\frac{\mathbb{G}}{\beta}\right) - y_F\right] N_{F,Max} \qquad \text{for DR-PH-A} \qquad (35)$$

Hence, the total number of moles that need to be compressed ($Comp$) for both of these configurations is the summation of the *actual* amount of gas that needs to be compressed to achieve the pressure swing and the heavy reflux supplied to the column undergoing the constant high pressure step:

$$N_{Comp} = \left(N_{Comp,PS} + N_{H,in}\right) \qquad (36)$$

It is important to note here that, even at constant values of P_L, $\mathbb{P}$, V_{bed}, ε, β_A, β, R, T and y_F, the calculated values of $Z_{F,opt}$, $\mathbb{G}$, $\mathbb{C}_{Max}$, and y^* (therefore the values $N_{F,Max}$, $N_{H,in}$, $\mathbb{H}$ and N_{Comp}) for both DR-PL-A and DR-PH-A process cycle configurations will differ from each other. This intentional corollary can be exploited to facilitate the selection between DR-PL-A and DR-PH-A process cycle configurations.

The two quantities $N_{F,Max}$ (maximum amount of feed that can be processed) and N_{Comp} (total number of moles that need to be compressed) can be comparatively evaluated for both DR-PL-A and DR-PH-A cycle configurations, while operating both the systems at optimal conditions ($Z_{F,opt}$ and $\mathbb{C}_{Max}$) for complete separation at CSS. In such a scenario, since the process input parameters (kind and amount of adsorbent, feed gas composition, operating temperature and pressure ratio) and process benchmarks (maximum adsorbent utilization and achievement of complete separation at CSS) remain identical for both configurations, the ratio $N_{F,Max}/N_{Comp}$ serves as a kind of *selection criterion* and facilitates choice amongst DR-PL-A and DR-PH-A configurations. Of course, higher values of this ratio correspond to higher amount of feed that can be processed $\left(N_{F,Max}\right)$ and lower amount of gas that needs to be compressed $\left(N_{Comp}\right)$ i.e. lower energy consumption.

http://dx.doi.org/10.1016/j.cej.2016.11.111

Let us discuss the effect of the input parameters (β, y_F and $\mathbb{P}$) on the two main operating variables ($Z_{F,opt}$ and $\mathbb{G}$), and on the selection criterion $\left(N_{F,Max}/N_{Comp}\right)$ defined above for both process cycle configurations. In all cases, maximum adsorbent utilization and complete separation at CSS (i.e. optimal conditions) will be considered. For ease of comparison, the maximum and minimum limits of both the axes are held constant in Fig. 6, 7 and 8.

Each simulation was carried out by varying $\mathbb{P}$ (from a maximum value of 10 to a minimum value), while setting different values of β and y_F (ranging from 0.1 to 0.9). In all cases, the minimum value of $\mathbb{P}$ was selected in order to ensure the full development of the shock in the *stripping wave* at the end of the cycle: this is of course needed to establish complete separation at CSS. Note that the computations carried out at smaller β values (0.1 and 0.3) for both process configurations either did not converge (due to incomplete shock development in the *stripping wave* at the end of the cycle) or converged for a range of $\mathbb{P}$ values that were different for each process cycle configuration. Such converged simulation results were deemed to be impractical for comparative assessment. Therefore, only the results obtained at β equal to $0.5, 0.7$ and 0.9 are discussed. Note that, at very low values of β (0.1 and 0.3), separation of feed gas mixture is feasible but complete separation is not attainable (at maximum adsorbent utilization) in majority of cases.

The variation of $Z_{F,opt}$ with respect to $\mathbb{P}$ for β equal to $0.5, 0.7$ and 0.9 and y_F equal to $0.1, 0.3, 0.5, 0.7$ and 0.9 is shown in Fig. 6 for both DR-PL-A and DR-PH-A. In all of these instances, it is evident that the optimal feed position values decrease as the value of $\mathbb{P}$ increases. For DR-PH-A cycle configuration, the influence of y_F on $Z_{F,opt}$ is negligible at high $\mathbb{P}$ values, whereas such influence gains some significance at lower $\mathbb{P}$ values, especially at low β values. Similar influence cannot be inferred for DR-PL-A cycle configuration. On the other hand, the values of $Z_{F,opt}$ are generally higher for DR-PL-A as compared to DR-PH-A cycle configuration. This difference is higher when higher $\mathbb{P}$ and β values are considered. Hence, with regard to

http://dx.doi.org/10.1016/j.cej.2016.11.111

the optimal feed position, DR-PL-A is more practical than DR-PH-A, especially while operating at higher $\mathbb{P}$ and β values.

Fig. 7 depicts the variation of $\mathbb{G}$ with respect to $\mathbb{P}$ for the same range of values for β and y_F considered in Fig. 6, again for both process cycle configurations. Note that, for better interpretation, the vertical axes of each of the charts are limited to $\mathbb{G} = 50$. For both (DR-PL-A and DR-PH-A) process cycle configurations, it is evident that the light recycle ratio values increase with decrease in $\mathbb{P}$; moreover, the sensitivity of $\mathbb{G}$ to the lower values of $\mathbb{P}$ is very large. Such sensitivity increases when adsorbent with lower selectivity (higher β) is chosen, thereby confirming that higher recycle ratios are needed for low selectivity adsorbents to achieve the same process performance when operating at given y_F and $\mathbb{P}$ values.

In order to facilitate the selection between DR-PL-A and DR-PH-A process cycle configurations, the quantities N_{Comp} (total number of moles that actually need to be compressed) and $N_{F,Max}$ (maximum amount of feed that can be processed) were evaluated at constant values of the parameters P_L, V_{bed}, ε, β_A, R, T, while operating the system at optimal conditions, i.e. $Z_{F,opt}$ and $\mathbb{C}_{Max}$. In order to avoid ambiguity, the specific values of the parameters were kept identical to those mentioned by Kearns and Webley [25]. Note that even if other values of these parameters were chosen, the individually computed values of $N_{F,Max}$ and N_{Comp} will differ but their ratio $\left(N_{F,Max}/N_{Comp}\right)$ will remain constant and equal to the one reported here when keeping constant the values of $\mathbb{P}$, β and y_F, as can be easily understood from the aforementioned equations. The variation of the ratio $N_{F,Max}/N_{Comp}$ with respect to $\mathbb{P}$, for the different values of β and y_F considered above, is shown in Fig. 8 for both DR-PL-A and DR-PH-A. In each of the charts depicted in Fig. 8, the ratio $\left(N_{F,Max}/N_{Comp}\right)$ tends to follow a peculiar trend at increasing $\mathbb{P}$: an initial surge followed by a gradual decline. This is essentially due to the two conflicting factors that come into play: (i) the direct proportionality of $N_{Comp,PS}$ to $\mathbb{P}$ (higher amount of gas needs to be compressed at higher operating pressure ratios), and (ii) the decrease of $\mathbb{G}$ with increase in $\mathbb{P}$ (cf. Fig. 7). Since $\mathbb{G} = \dot{N}_{L,in}/\dot{N}_F$, higher $N_{L,in}$ (and consequently higher $N_{H,in}$) and/or lower N_F are encountered at lower $\mathbb{P}$

http://dx.doi.org/10.1016/j.cej.2016.11.111

values, and vice versa. This peculiar trend of the ratio $\left(N_{F,Max}/N_{Comp}\right)$ encounters a peak at certain $\mathbb{P}$. Such specific $\mathbb{P}$ can be termed as the "optimal operating pressure ratio" and, for every curve, it lies within the shaded portion of the charts depicted in Fig. 8.

From all the results shown in Fig. 8, the following guidelines can be drawn:

1) For both of the process cycle configurations, adsorbents with higher selectivity (lower β value) are able to process higher amount of feed at lower expense of energy;
2) DR-PL-A process cycle configuration should be selected only when feed gas with $y_F \geq 0.9$ needs to be processed. For all other y_F values, DR-PH-A should be selected while operating at lower $\mathbb{P}$;

For a given value of $\mathbb{P}$, the calculated value of $\mathbb{G}$ increases (and consequently $N_{H,in}$ increases and/or N_F decreases) with increase in the value of β (cf. Fig. 7). Such combined effect leads to: (i) higher amount of feed being processed at lower expense of energy for adsorbents with lower β (higher selectivity), and (ii) the shift of the shaded region (optimal operating pressure ratio range) towards higher $\mathbb{P}$ values with reduction in adsorbent selectivity (higher β value).

4. Conclusions

To simulate the complete separation of binary feed gas mixtures at cyclic steady state conditions (CSS), an equilibrium theory based model, previously reported for DR-PSA and limited to DR-PH-A process configuration, was extended to the process configuration DR-PL-A. Additionally, an in-depth analysis of the impact of the process parameters (β, y_F and $\mathbb{P}$) on key operating variables ($Z_{F,opt}$ and $\mathbb{G}$), and a suitably defined selection criterion $\left(N_{F,Max}/N_{Comp}\right)$ is comparatively discussed for both process cycle configurations. With respect to previous literature, following major accomplishments can be mentioned:

(i) The proposed modeling approach provides unique insights into the separation behavior of the DR-PL-A process cycle configuration;

http://dx.doi.org/10.1016/j.cej.2016.11.111

(ii) Vital design constraints needed to establish complete separation at CSS in DR-PL-A process cycle configuration are elaborated;

(iii) An optimal design strategy for DR-PL-A units has been formulated. It identifies a triangular operating region, inside which, complete separation at CSS can be achieved. This complete separation region establishes a clear correlation between the specific value of Z_F (proposed by Kearns and Webley [7] for maximum adsorbent utilization) and its feasible range of values (from minimum $(Z_{F,Min})$ to maximum $(Z_{F,Max})$, put forth by Ebner and Ritter [23]);

(iv) A procedure to evaluate the optimal values of feed position $(Z_{F,opt})$ as well as other relevant operating variables has been developed, where optimality is defined in terms of best use of adsorbent;

(v) A novel selection criterion that facilitates choice amongst DR-PL-A and DR-PH-A process cycle configurations has been presented;

(vi) The optimal operating pressure ratio range for both the process cycle configurations has been discussed.

Notes

This research did not receive any specific grant from funding agencies in the public, commercial, or not-for-profit sectors.

http://dx.doi.org/10.1016/j.cej.2016.11.111

Appendices

Appendix A: Numerical approach

For calculating the composition profiles as well as the evolution of SW and RW during the four steps of the DR-PL-A process cycle, an equilibrium theory based numerical code was developed in Matlab®. Within suitable grids of space and time (or pressure) values, the trajectory of each characteristic all along the unit bed is numerically tracked. When the program detects that the adjacent characteristics have "crossed-over", it applies corresponding shock equations to evaluate the resulting concentration values.

Given specific values of separation parameter of the adsorbent (β), pressure ratio ($\mathbb{P}$), and feed composition (y_F), the operating parameters feed position (Z_F), starting position of RW (Z^*), capacity ratio of the *purge* step ($\mathbb{C}$), and light recycle ratio ($\mathbb{G}$) are evaluated as explained in section 5 as corresponding to optimal conditions (i.e., maximum adsorbent utilization and achievement of complete separation at CSS). In particular, we found especially convenient to guess $Z_{F,opt}$ and calculate the corresponding values of $\mathbb{G}, \mathbb{C}_{Max}$ and Z^* through Eq. (29), (30) and the limiting value of inequality (25), respectively. Specifically, the "correct" value of $Z_{F,opt}$ should ensure that the shocks in the *stripping* and *rectifying* waves reach their respective positions at the end of the *purge* step, $Z = 0$ and $Z = Z^*$, in a fully developed form ($y_1 = y^*$, $y_2 = 0$ for SW and $y_1 = 1$, $y_2 = y^*$ for RW). It was observed that the correct value of the optimum feed position $Z_{F,opt}$ can be estimated by checking the fulfillment of the previous constraint for one single wave, SW or RW, being the fulfillment of the same condition for the other wave automatic. Finally, it is important here to note that complete shock development in the *stripping* wave may not be possible at lower values of β (separation parameter of the adsorbent) and/or pressure ratio ($\mathbb{P}$) and/or feed composition (y_F), i.e. complete separation is not always possible at CSS.

http://dx.doi.org/10.1016/j.cej.2016.11.111

Appendix B: Utilizing the triangular operating zone to demonstrate the optimal design strategy of DR-PSA units that employ DR-PL-A process cycle configuration

The Triangular Operating Zone (TOZ) was evaluated at constant values of y_F, β and $\mathbb{P}$ ($y_F = 0.5, \beta = 0.5$ and $\mathbb{P} = 1.5$) and simulations at different pairs of $Z_F, \mathbb{C}$ values were performed using the numerical code (described in *Appendix A*) to prove: (i) the optimal design strategy, and; (ii) that complete separation at CSS can be achieved at different feed positions within the TOZ. The evaluated TOZ is depicted in Fig. B1 and the distinct pairs of $Z_F, \mathbb{C}$ values, selected for performing simulations, are signposted as *Test-A* to *Test-D*.

The process benchmarks: maximum adsorbent utilization and complete separation at CSS; can be accomplished *only* while operating the system at $Z_{F,opt}$ and $\mathbb{C}_{Max}$, i.e. *Test-A*. The corresponding composition profiles during all the four steps of the cyclic process are depicted in Fig. B2. As evident from the composition profiles for this test, there is no constant composition plateau that moves back and forth during the four steps of the cycle without contributing to the separation process, subsequently ensuring minimum solid requirement per mole of feed (i.e. maximum utilization of the adsorbent).

Three distinct values of the feed position ($Z_{F,Min}$, $Z_{F,Max}$ and $Z_{F,opt}$) but an identical value of $\mathbb{C} < \mathbb{C}_{Max}$ was considered for *Test-B* to *Test-D*. As depicted in Fig. B1, the system was operated at $Z_{F,Min}$ and $\mathbb{C}$ while performing *Test-B*. The resulting composition profiles are shown in Fig. B3. The unutilized adsorbent (depicted by shaded region) in the *rectifying section* of the column is the consequence of a constant composition plateau at $y = 1$ that moves back and forth but, it doesn't contribute to the actual separation of gases during the four steps of the cyclic process. While performing *Test-C* however, the system was operated at $Z_{F,Max}$ and $\mathbb{C}$. The composition profiles for this particular test are shown in Fig. B4. It depicts a concentration plateau in the *stripping section* of the column which moves back and forth during the four steps of the cycle without contributing to the separation process: therefore, some volume of adsorbent will remain unutilized in the *stripping section* of the column (displayed as the shaded region in Fig. B4).

http://dx.doi.org/10.1016/j.cej.2016.11.111

Finally, the system was operated at an intermediate feed position ($Z_{F,Min} < Z_{F,opt} < Z_{F,Max}$) and $\mathbb{C}$ while performing *Test-D*. The resulting composition profiles are shown in Fig. B5. Some adsorbent remained unutilized in both (the *stripping* as well as the *rectifying*) column sections, as shown by the shaded regions in Fig. B5. This necessarily results from the fact that both of these sections contain a concentration plateau that does not contribute to the separation process. Even though complete separation at CSS will be achieved in *Test-B* to *Test-D*; the deliberate selection of $\mathbb{C} < \mathbb{C}_{Max}$ resulted in unutilized portions of adsorbent. Such operation reduces the process productivity; however, it also improves the process robustness by ensuring either one or both of these possibilities: (i) pure A is injected-in and pushed-out of the *Rectifying Section* end, $Z = 1$; (ii) a feeding zone is available in the *stripping section* of the column.

http://dx.doi.org/10.1016/j.cej.2016.11.111

References

[1] T. Hirose, A simple design method of a new PSA process consisting of both rectifying and stripping sections. In Proceedings of the 2nd China-Japan-USA Symposium on Adsorption (1991) Vol. 123.

[2] F.W. Leavitt, Duplex Adsorption Process. US Patent 5,085,674 (1992).

[3] C.W. Skarstrom, Use of adsorption phenomena in automatic plant-type gas analysers. Annals of the New York Academy of Sciences 72 (1959), 751–763.

[4] M. Yoshida, J.A. Ritter, A. Kodama, M. Goto, T. Hirose, Enriching reflux and parallel equalization PSA process for concentrating trace components in air. Industrial and Engineering Chemistry Research 42 (2003), 1795-1803.

[5] D. Diagne, M. Goto, T. Hirose, New PSA Process with Intermediate Feed Inlet Position Operated with Dual Refluxes: Application to Carbon Dioxide Removal and Enrichment. Journal of chemical engineering of Japan, 27(1), 1994, pp.85-89.

[6] A.D. Ebner, J.A. Ritter, Equilibrium theory analysis of rectifying PSA for heavy component production. AIChE journal, 48(8), 2002, pp.1679-1691.

[7] D.T. Kearns, P.A. Webley, Modelling and evaluation of dual-reflux pressure swing adsorption cycles: Part I. Mathematical models. Chemical engineering science, 61(22), 2006, pp.7223-7233.

[8] D. Diagne, M. Goto, T. Hirose, Experimental study of simultaneous removal and concentration of CO2 by an improved pressure swing adsorption process. Energy conversion and management, 36(6), 1995, pp.431-434.

[9] D. Diagne, M. Goto, T. Hirose, Parametric studies on CO2 separation and recovery by a dual reflux PSA process consisting of both rectifying and stripping sections. Industrial & Engineering Chemistry

http://dx.doi.org/10.1016/j.cej.2016.11.111

Research, 34(9), 1995, pp.3083-3089.

[10] J.A. McIntyre, C.E. Holland, J.A. Ritter, High enrichment and recovery of dilute hydrocarbons by dual-reflux pressure-swing adsorption. Industrial & engineering chemistry research, 41(14), 2002, pp.3499-3504.

[11] J.A. McIntyre, A.D. Ebner, J.A. Ritter, Experimental study of a dual reflux enriching pressure swing adsorption process for concentrating dilute feed streams. Industrial & Engineering Chemistry Research, 49(4), 2010, pp.1848-1858.

[12] T.S. Bhatt, A. Sliepcevich, G. Storti, R. Rota, Experimental and Modeling Analysis of Dual-Reflux Pressure Swing Adsorption Process. Industrial & Engineering Chemistry Research, 53(34), 2014, pp.13448-13458.

[13] T.L. Saleman, G.K. Li, T.E. Rufford, P.L. Stanwix, K.I. Chan, S.H. Huang, E.F. May, Capture of low grade methane from nitrogen gas using dual-reflux pressure swing adsorption. Chemical Engineering Journal, 281 (2015), pp.739-748.

[14] D. Li, Y. Zhou, Y. Shen, W. Sun, Q. Fu, H. Yan, D. Zhang, Experiment and simulation for separating CO2/N2 by dual-reflux pressure swing adsorption process. Chemical Engineering Journal, 297 (2016), pp.315-324.

[15] D. Diagne, M. Goto, T. Hirose, Numerical analysis of a dual refluxed PSA process during simultaneous removal and concentration of carbon dioxide dilute gas from air. Journal of Chemical Technology and Biotechnology, 65(1), 1996, pp.29-38.

[16] G. Spoorthi, R.S. Thakur, N. Kaistha, D.P. Rao, Process intensification in PSA processes for upgrading synthetic landfill and lean natural gases. Adsorption, 17(1), 2011, pp.121-133.

[17] R.S. Thakur, N. Kaistha, D.P. Rao, Process intensification in duplex pressure swing adsorption.

http://dx.doi.org/10.1016/j.cej.2016.11.111

Computers and Chemical Engineering 35 (2011), 973–983.

[18] S.V. Sivakumar, D.P. Rao, Modified Duplex PSA. 1. Sharp separation and process intensification for CO2− N2− 13X zeolite system. Industrial & Engineering Chemistry Research, 50(6), 2011, pp.3426-3436.

[19] S.V. Sivakumar, D.P. Rao, Modified Duplex PSA. 2. Sharp separation and process intensification for N2-O2-5A zeolite system. Industrial & Engineering Chemistry Research, 50(6), 2011, pp.3437-3445.

[20] T.S. Bhatt, G. Storti, R. Rota, Detailed simulation of dual-reflux pressure swing adsorption process. Chemical Engineering Science, 122 (2015), pp.34-52.

[21] Y. Zhang, T.L. Saleman, G.K. Li, G. Xiao, B.R. Young, E.F. May, Non-isothermal numerical simulations of dual reflux pressure swing adsorption cycles for separating N2 + CH4. Chemical Engineering Journal, 292 (2016), pp.366-381.

[22] H.K. Rhee, R. Aris, N.R. Amundson, First-order partial differential equations, Vol. 1. Prentice-Hall, Englewood Cliffs, N.J. (1986)

[23] A.D. Ebner, J.A. Ritter, Equilibrium theory analysis of dual reflux PSA for separation of a binary mixture. AIChE journal, 50(10), 2004, pp.2418-2429.

[24] T.S. Bhatt, G. Storti, R. Rota, Optimal design of dual-reflux pressure swing adsorption units via equilibrium theory. Chemical Engineering Science, 102 (2013), pp.42-55.

[25] D.T. Kearns, P.A. Webley, Modelling and evaluation of dual reflux pressure swing adsorption cycles: Part II. Productivity and energy consumption. Chemical engineering science, 61(22), 2006, pp.7234-7239.

[26] A.S. Chiang, An analytical solution to equilibrium PSA cycles. Chemical engineering science, 51(2), 1996, pp.207-216.

http://dx.doi.org/10.1016/j.cej.2016.11.111

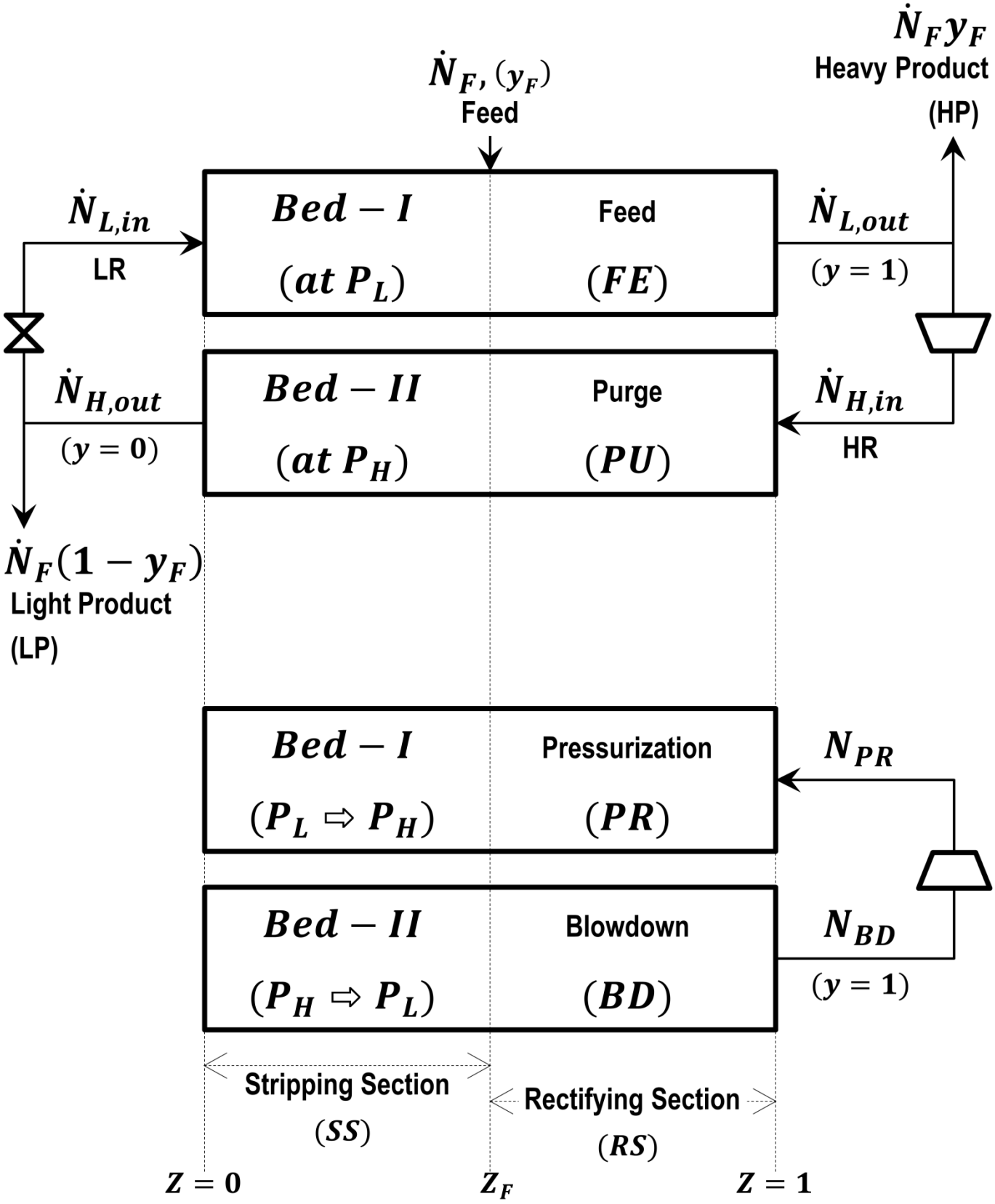

Fig. 1. Cycle steps and flows of a typical DR-PL-A process cycle configuration for complete separation at CSS.

http://dx.doi.org/10.1016/j.cej.2016.11.111

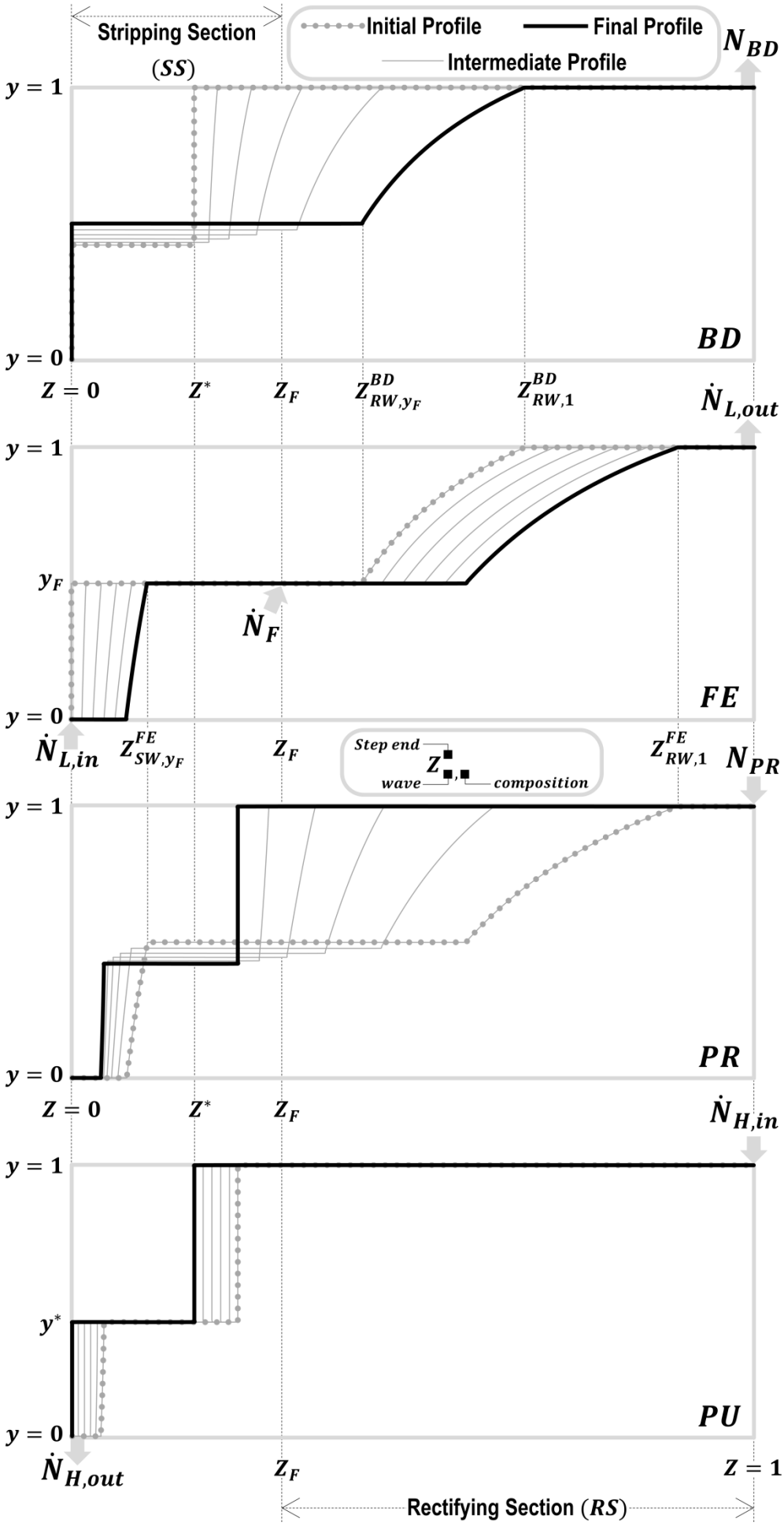

Fig. 2. Composition profiles for DR-PL-A process cycle configuration during the four steps of the cyclic process, for complete separation at CSS.

http://dx.doi.org/10.1016/j.cej.2016.11.111

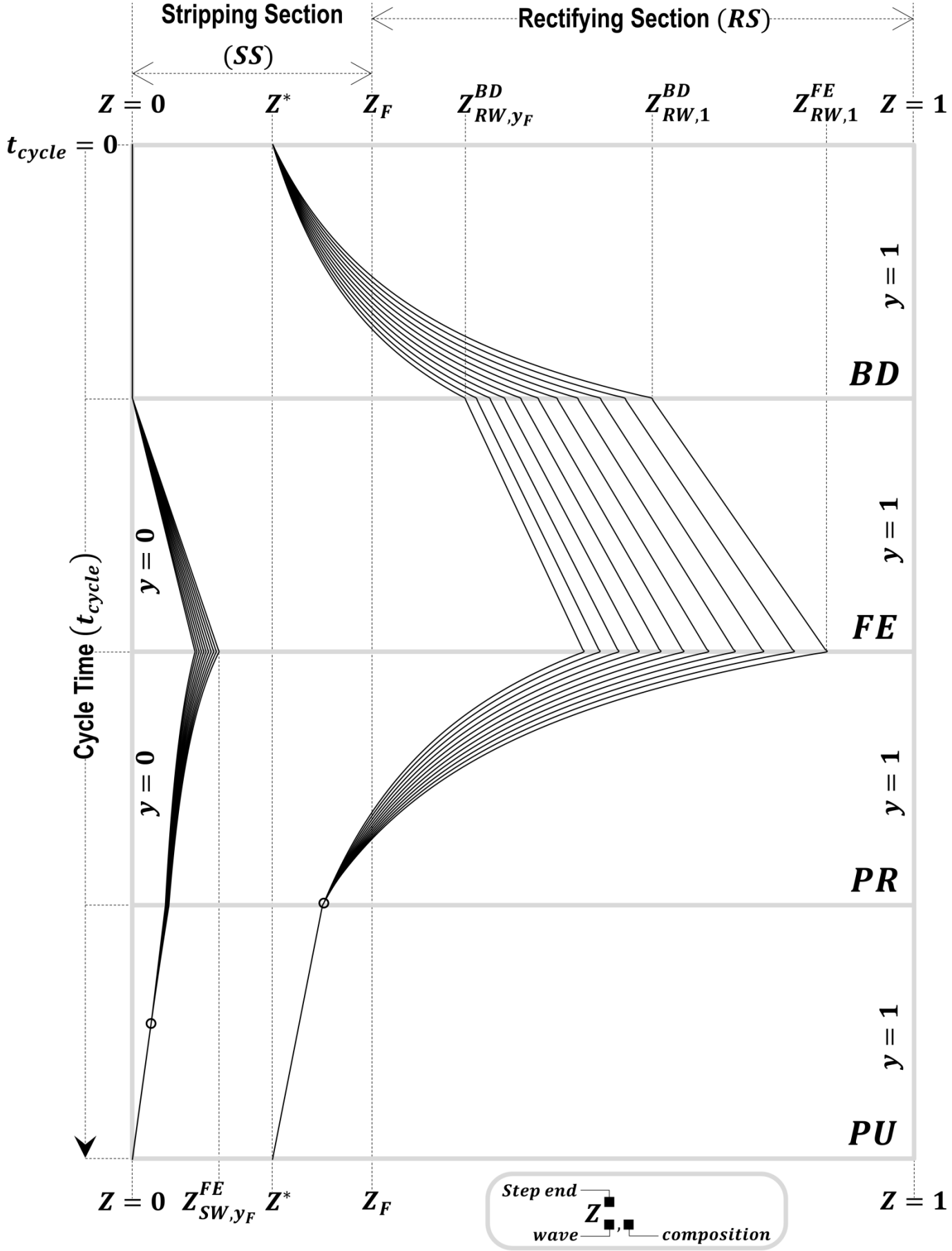

Fig. 3. Trajectory of waves/shocks in both sections of a column for DR-PL-A process cycle configuration during the four steps of the cyclic process, for complete separation at CSS.

http://dx.doi.org/10.1016/j.cej.2016.11.111

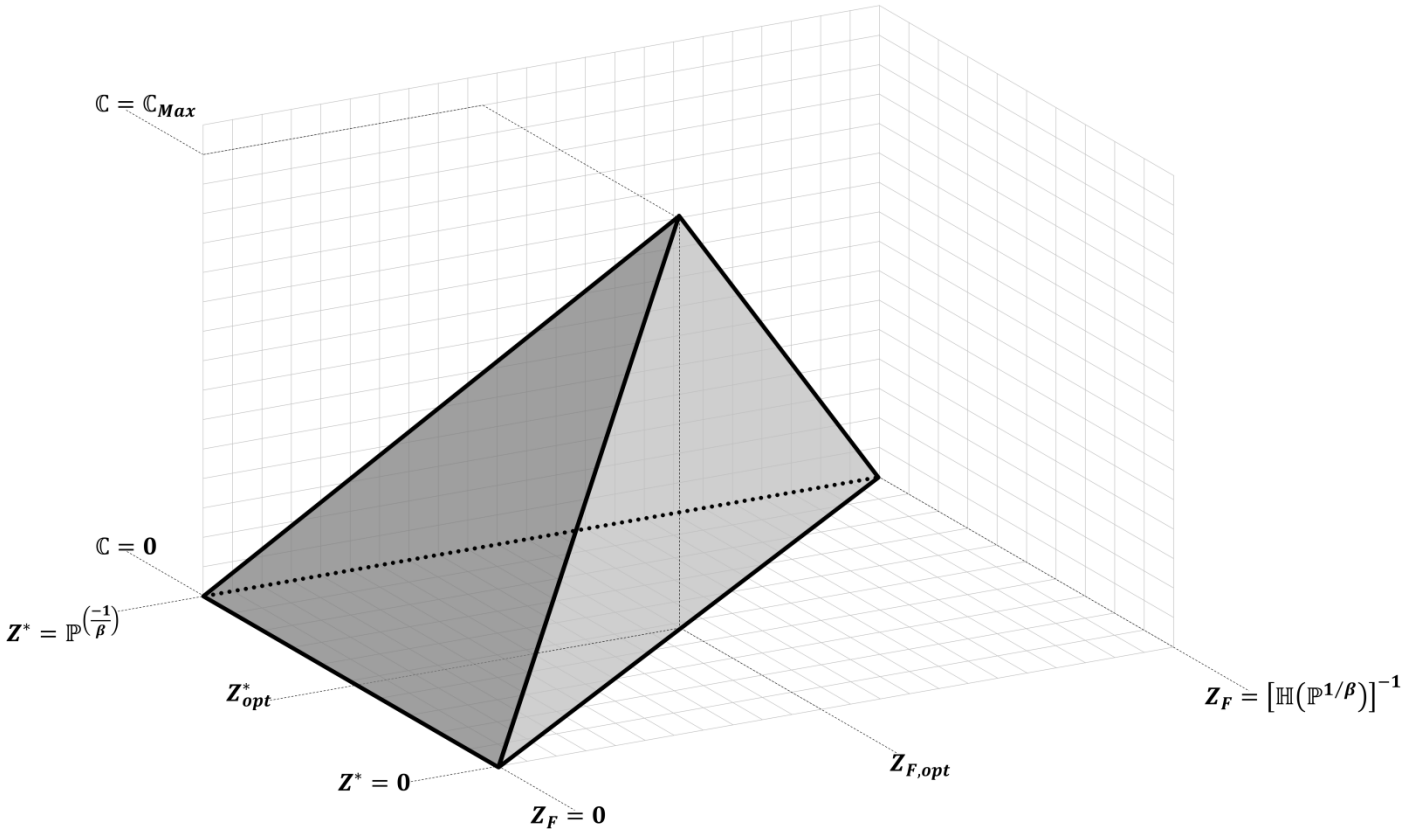

Fig. 4a. Qualitative representation of the tetrahedron plotted in $(Z_F - Z^* - \mathbb{C})$ space.

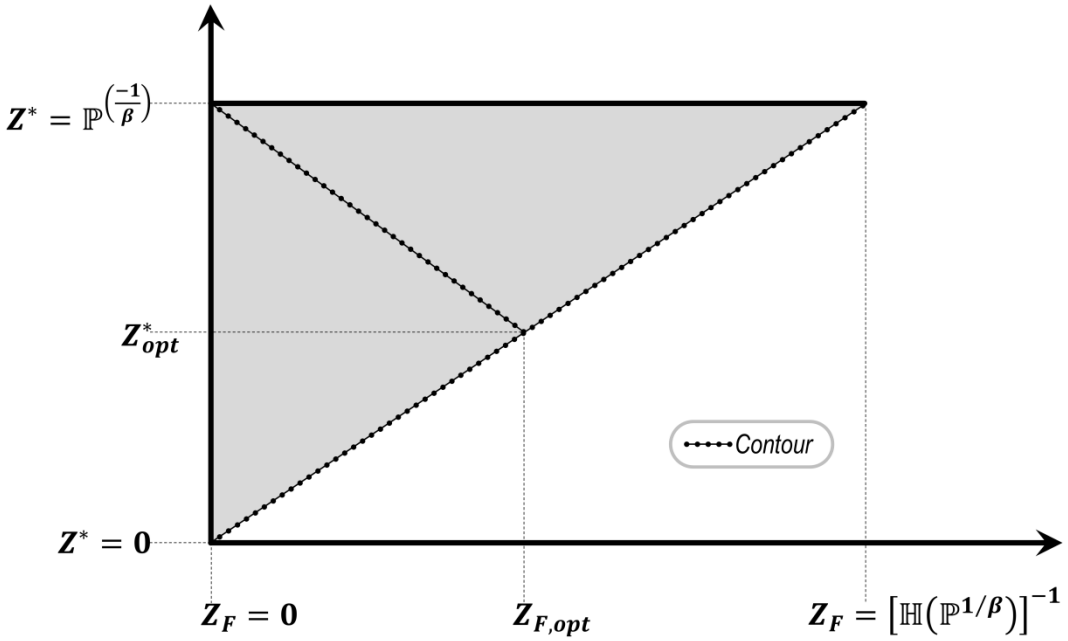

Fig. 4b. Top view (plotted in $Z_F - Z^*$ plane) of the tetrahedron.

http://dx.doi.org/10.1016/j.cej.2016.11.111

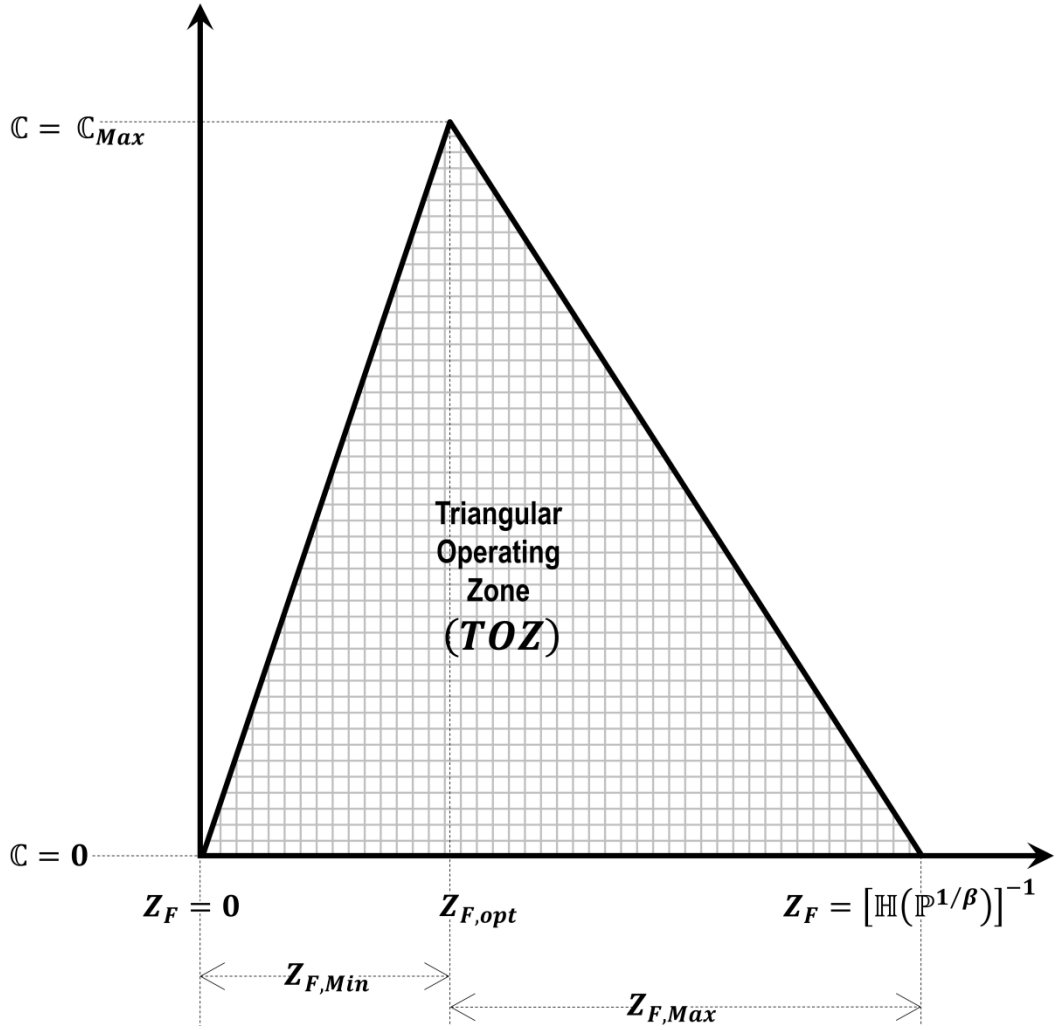

Fig. 5. Qualitative representation of 'Triangular Operating Zone' (checkered region).

http://dx.doi.org/10.1016/j.cej.2016.11.111

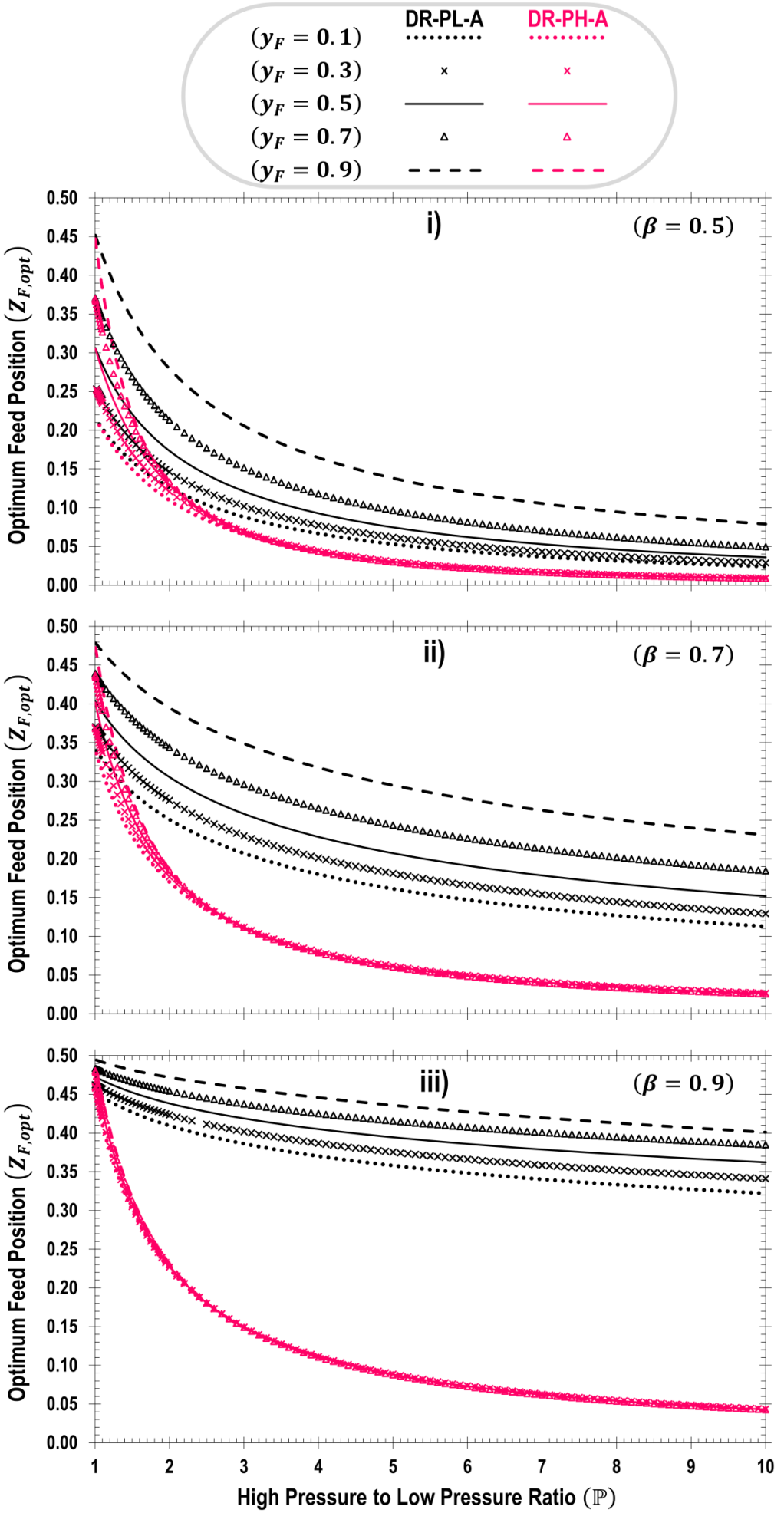

Fig. 6. $\mathbb{P}$ versus $Z_{F,opt}$ in DR-PL-A and DR-PH-A process cycle configurations, for: β equal to $0.5, 0.7$ and 0.9 and; y_F equal to $0.1, 0.3, 0.5, 0.7$ and 0.9.

http://dx.doi.org/10.1016/j.cej.2016.11.111

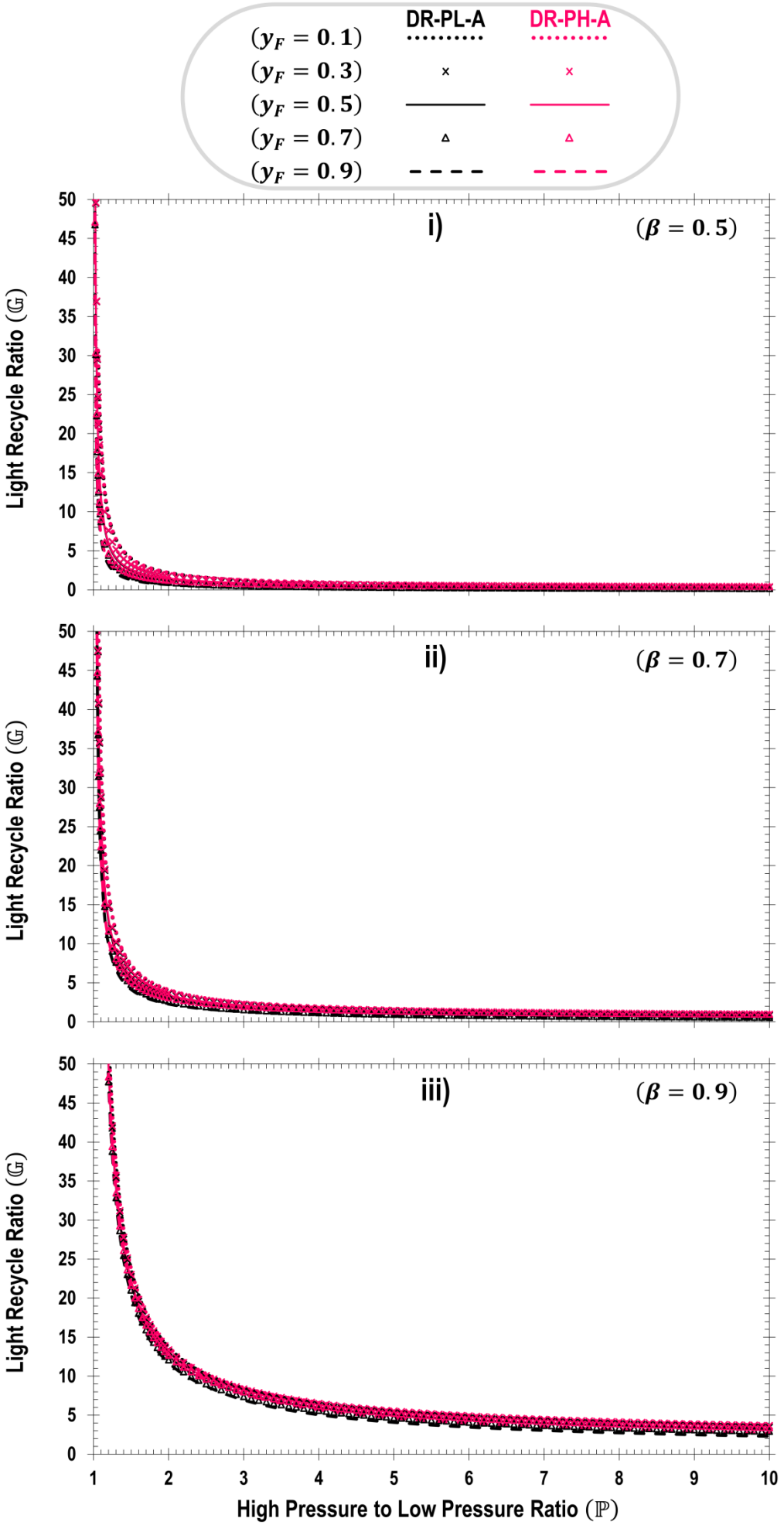

Fig. 7. $\mathbb{P}$ versus $\mathbb{G}$ in DR-PL-A and DR-PH-A process cycle configurations, for: β equal to $0.5, 0.7$ and 0.9 and; y_F equal to $0.1, 0.3, 0.5, 0.7$ and 0.9.

http://dx.doi.org/10.1016/j.cej.2016.11.111

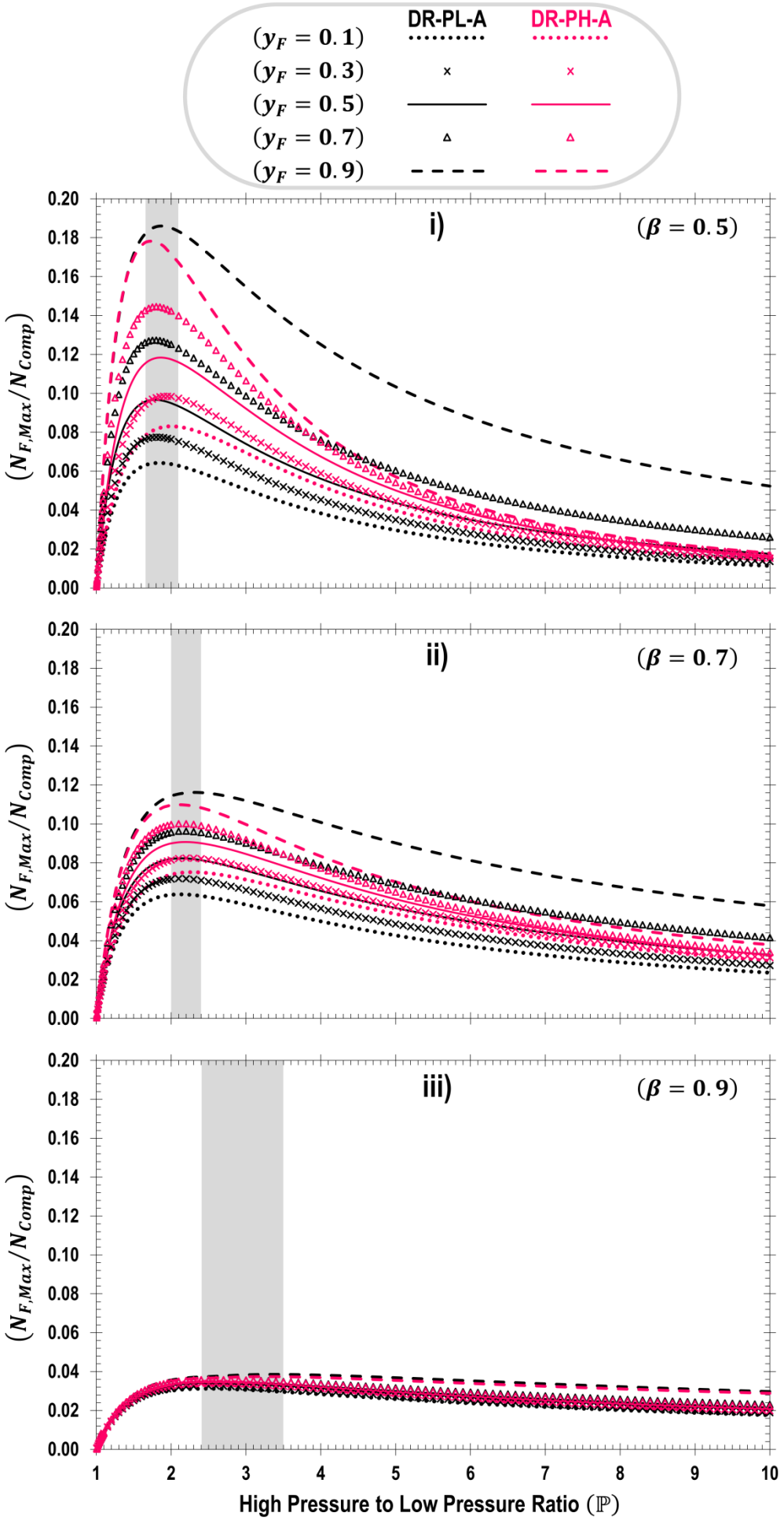

Fig. 8. $\mathbb{P}$ versus $(N_{F,Max}/N_{Comp})$ in DR-PL-A and DR-PH-A process cycle configurations, for: β equal to 0.5, 0.7 and 0.9 and; y_F equal to 0.1, 0.3, 0.5, 0.7 and 0.9. The shaded regions represent the optimal high to low operating pressure ratio range.

http://dx.doi.org/10.1016/j.cej.2016.11.111

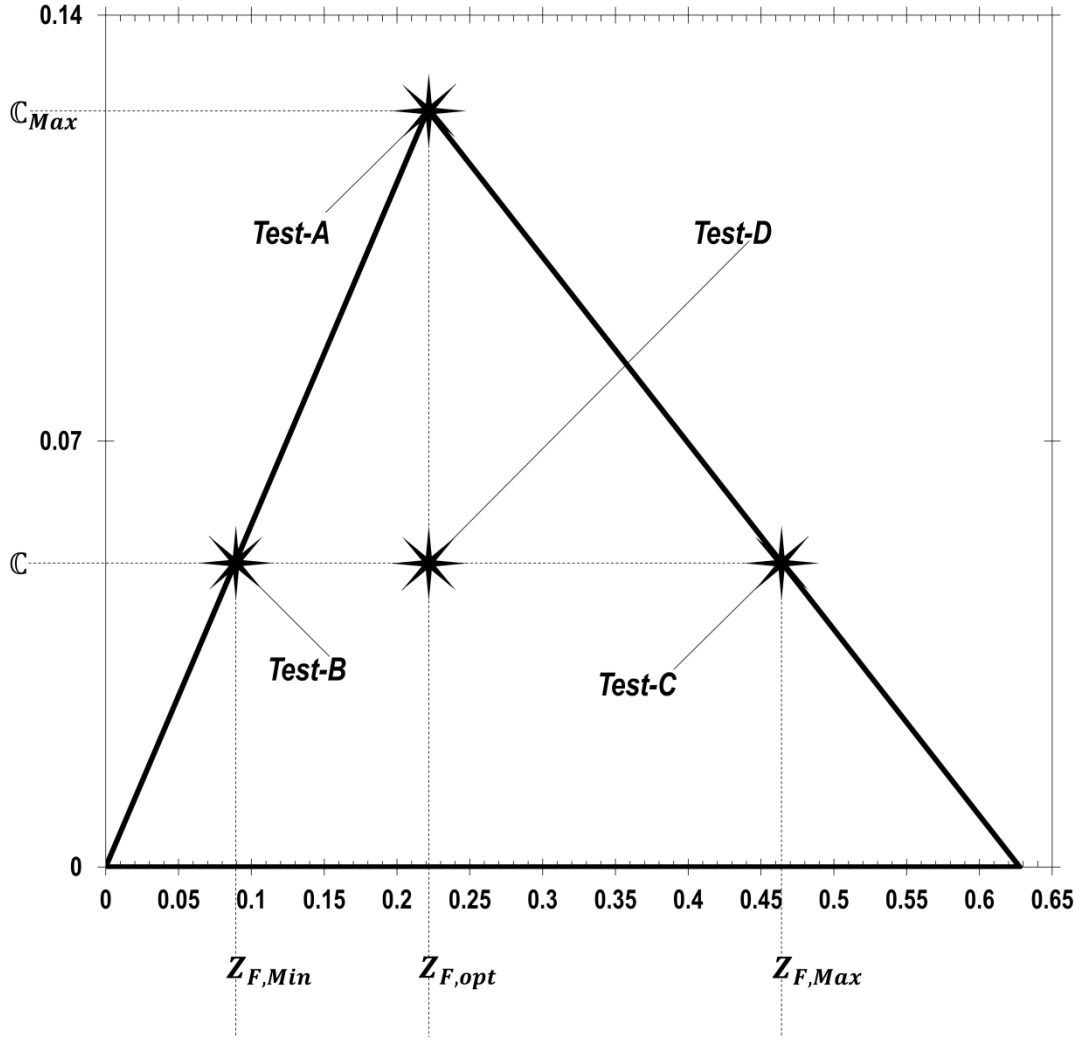

Fig. B1. Triangular Operating Zone (TOZ) for: $(y_F = 0.5)$, $(\beta = 0.5)$ and $(\mathbb{P} = 1.5)$.

http://dx.doi.org/10.1016/j.cej.2016.11.111

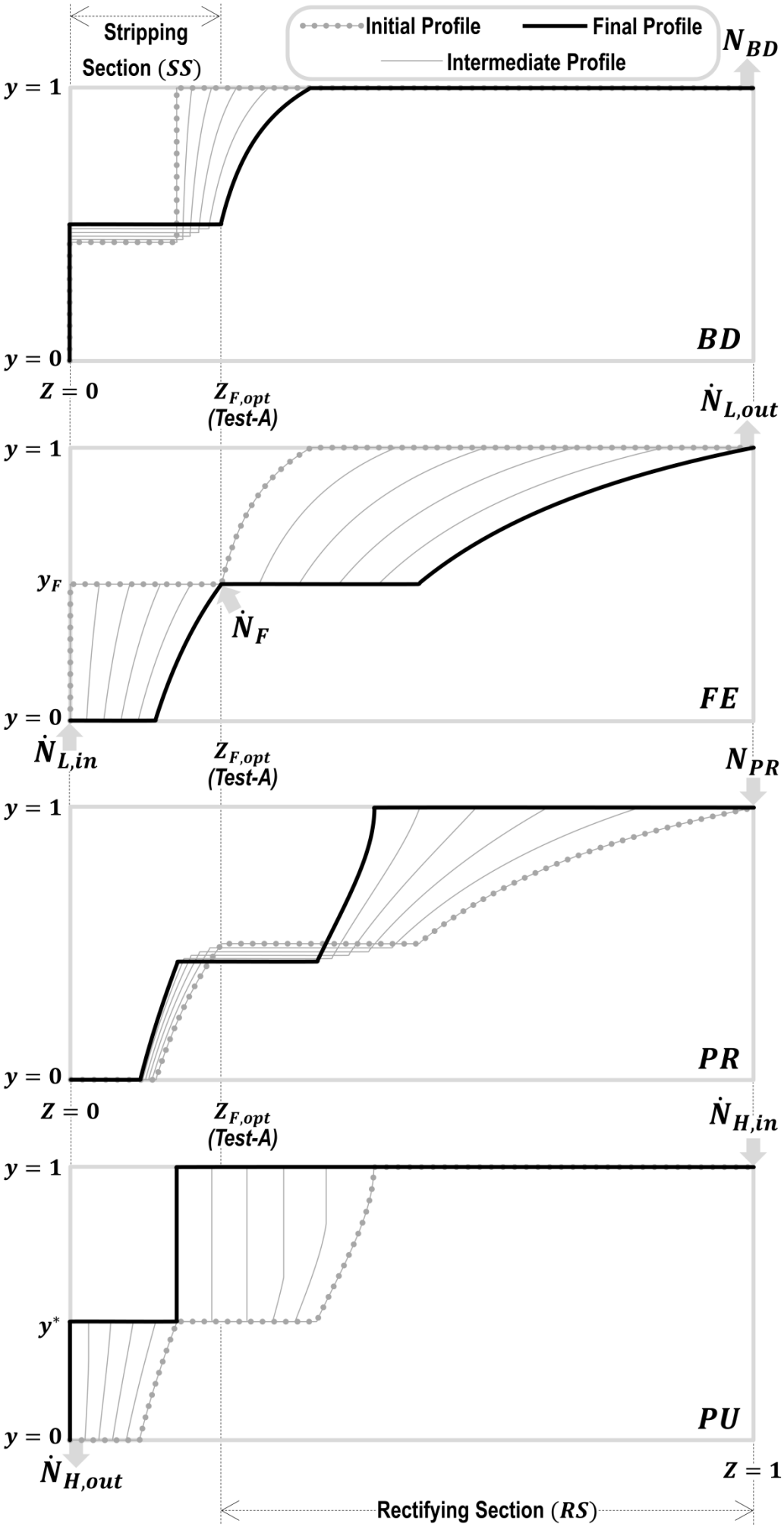

Fig. B2. Composition profiles for *Test-A* depicted in Triangular Operating Zone (TOZ of Fig. B1).

http://dx.doi.org/10.1016/j.cej.2016.11.111

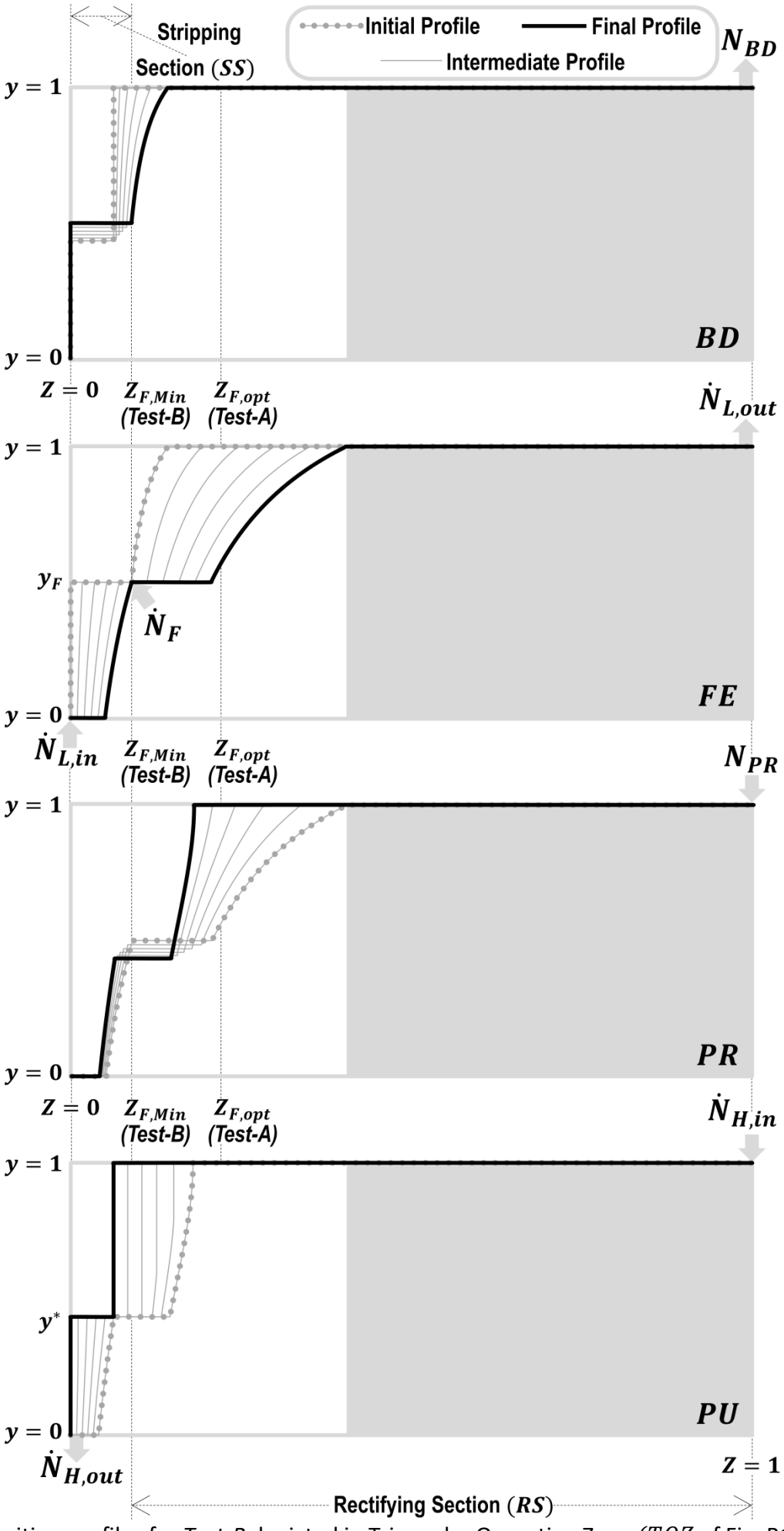

Fig. B3. Composition profiles for *Test-B* depicted in Triangular Operating Zone (TOZ of Fig. B1). The shaded portion represents the unutilized region of the bed.

http://dx.doi.org/10.1016/j.cej.2016.11.111

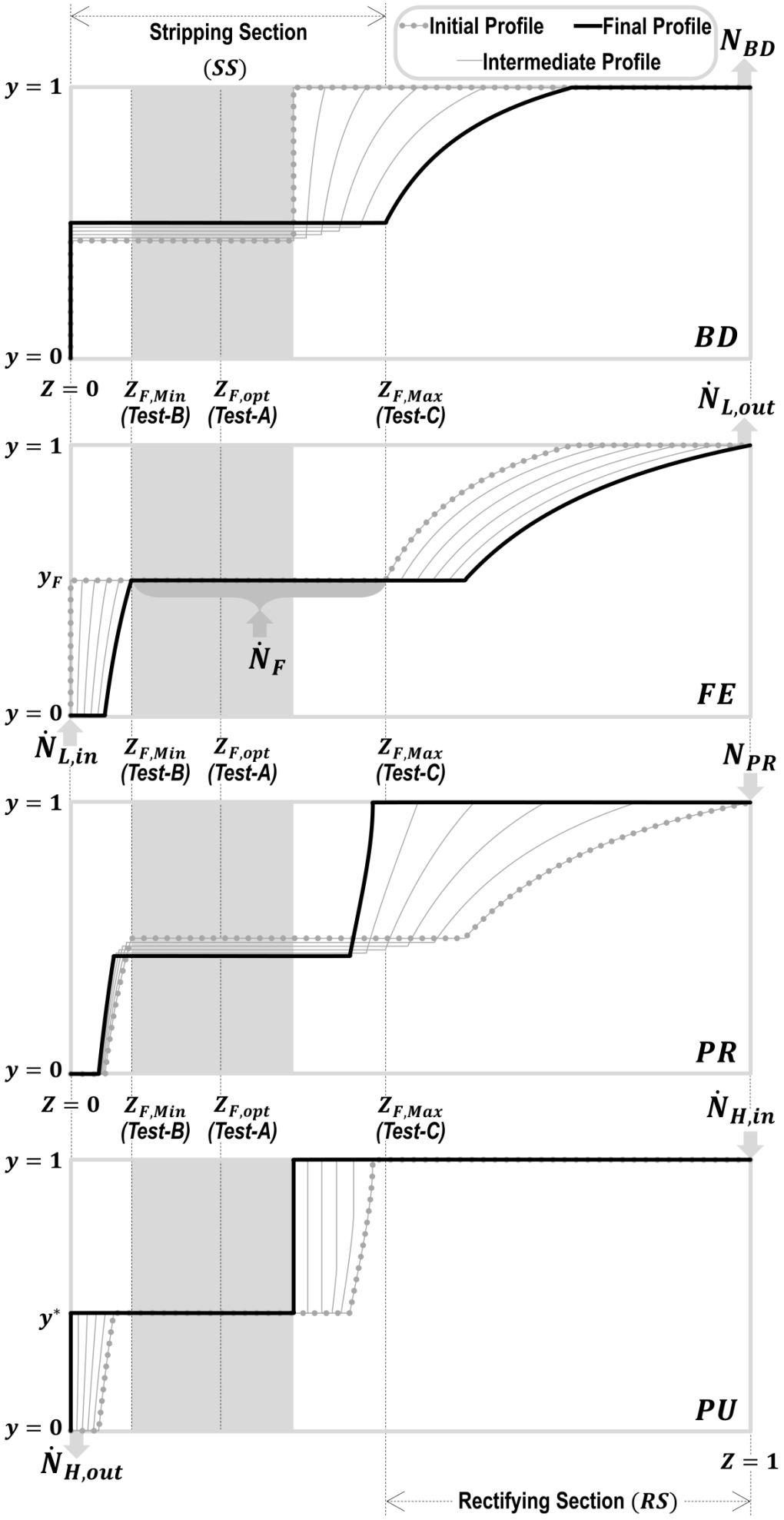

Fig. B4. Composition profiles for *Test-C* depicted in Triangular Operating Zone (TOZ of Fig. B1). The shaded portion represents the unutilized region of the bed.

http://dx.doi.org/10.1016/j.cej.2016.11.111

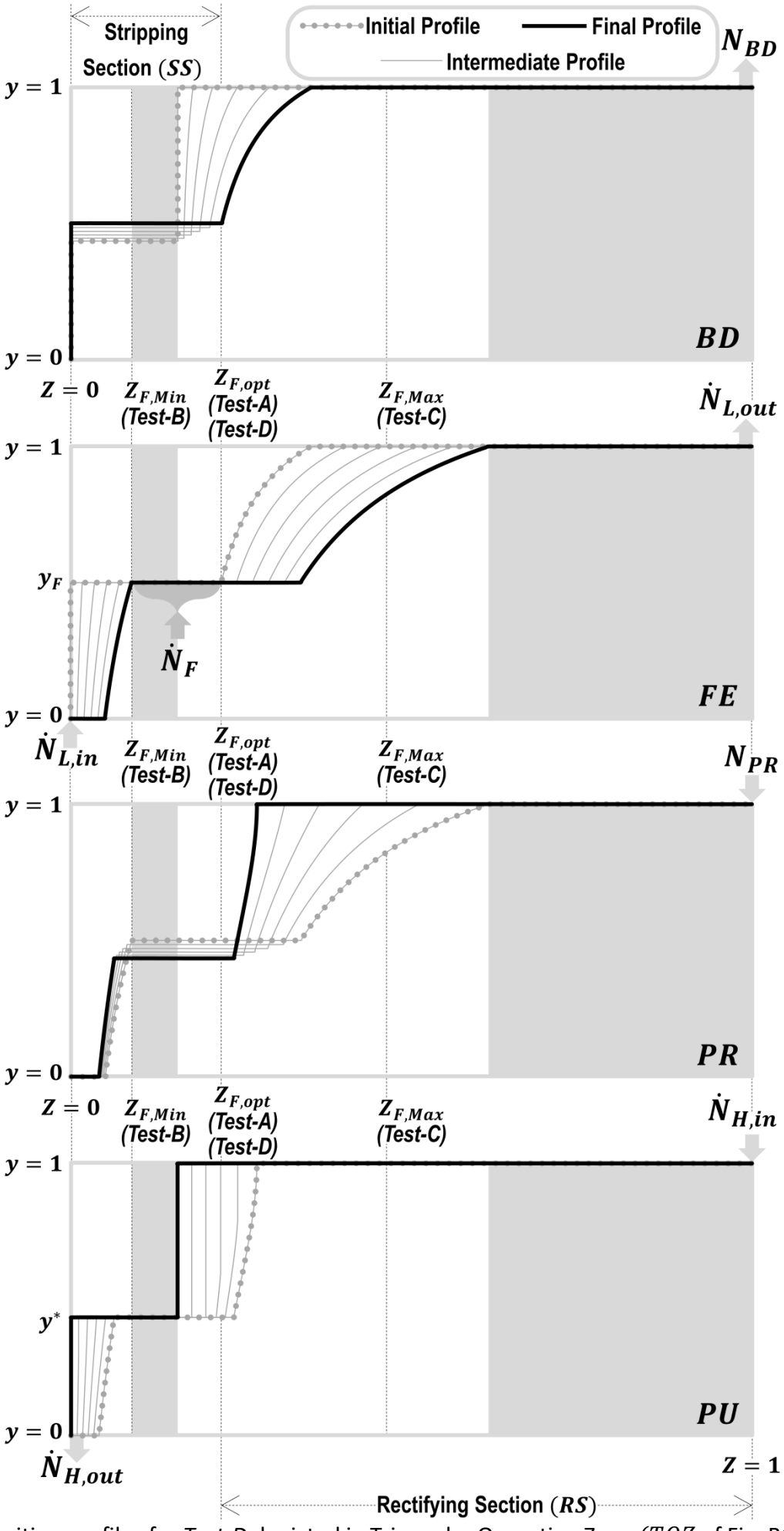

Fig. B5. Composition profiles for *Test-D* depicted in Triangular Operating Zone (TOZ of Fig. B1). The shaded portion represents the unutilized regions of the bed.

http://dx.doi.org/10.1016/j.cej.2016.11.111